การหาปริมาณรังสียังผลจากนิวตรอนและโฟตอนกระเจิงใน 3D, IMRT และ VMAT

นายอิศรา อิศรางกูร ณ อยุธยา

วิทยานิพนธ์นี้เป็นส่วนหนึ่งของการศึกษาตามหลักสูตรปริญญาวิศวกรรมศาสตรดุษฎีบัณฑิต
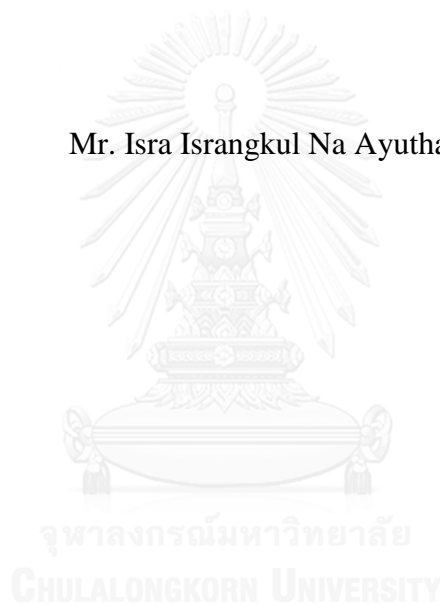สาขาวิชาวิศวกรรมนิวเคลียร์ ภาควิชาวิศวกรรมนิวเคลียร์
คณะวิศวกรรมศาสตร์ จุฬาลงกรณ์มหาวิทยาลัย
ปีการศึกษา 2557
ลิขสิทธิ์ของจุฬาลงกรณ์มหาวิทยาลัย

Determination of Effective Dose from Neutrons and Scatter photons in 3D, IMRT and VMAT

Mr. Isra Israngkul Na Ayuthaya

จุฬาลงกรณ์มหาวิทยาลัย
CHULALONGKORN UNIVERSITY

A Dissertation Submitted in Partial Fulfillment of the Requirements

for the Degree of Doctor of Engineering Program in Nuclear Engineering

Department of Nuclear Engineering

Faculty of Engineering

Chulalongkorn University

Academic Year 2014

Thesis Title   Determination of Effective Dose from Neutrons and Scatter photons in 3D, IMRT and VMAT

By   Mr. Isra Israngkul Na Ayuthaya

Field of Study   Nuclear Engineering

Thesis Advisor   Dr.Phongphaeth Pengvanich

Thesis Co-Advisor   Associate Professor Sivalee Suriyapee

Accepted by the Faculty of Engineering, Chulalongkorn University in Partial Fulfillment of the Requirements for the Doctoral Degree

- Dean of the Faculty of Engineering
(Associate Professor Dr.Sunchai Nilsuwankosit)

THESIS COMMITTEE

- Chairman
(Associate Professor Dr.Sunchai Nilsuwankosit)

- Thesis Advisor
(Dr.Phongphaeth Pengvanich)

- Thesis Co-Advisor
(Associate Professor Sivalee Suriyapee)

- Examiner
(Associate ProfessorSomyot Srisatit)

- External Examiner
(Dr.Puangpen Tungboonduangjit)

อิศรา อิศรางกูร ณ อยุธยา : การหาปริมาณรังสียังผลจากนิวตรอนและโฟตอนกระเจิงใน 3D, IMRT และ VMAT (Determination of Effective Dose from Neutrons and Scatter photons in 3D, IMRT and VMAT) อ.ที่ปรึกษาวิทยานิพนธ์หลัก: ดร.พงษ์แพทย์ เพ่งวาณิชย์, อ.ที่ปรึกษาวิทยานิพนธ์ร่วม: รศ. ศิวลี สุริยาปี, 82 หน้า.

รังสีโฟตอนกระเจิงและนิวตรอนที่เกิดจากรังสีโฟตอนพลังงานสูงกว่า 10 เมกะอิเล็กตรอนโวล์ทจะเพิ่มปริมาณรังสีที่ไม่พึงประสงค์ต่อผู้ป่วยและเจ้าหน้าที่ปฏิบัติงานในห้องฉายรังสีแบบเครื่องเร่งอนุภาค รังสีไม่พึงประสงค์นี้จะเกิดขึ้นภายนอกบริเวณลำรังสีที่ฉายให้ผู้ป่วย ซึ่งสามารถเพิ่มโอกาสในการเกิดโรคมะเร็งแบบทุติยภูมิได้ วัตถุประสงค์ของการศึกษานี้ เพื่อประเมินปริมาณรังสีสมมูลโฟตอนกระเจิงและนิวตรอนจากเทคนิคการฉายรังสี 3 เทคนิค คือ เทคนิคการฉายรังสีแบบ 3 มิติ แบบปรับความเข้ม (IMRT) และแบบปรับความเข้มหมุนรอบตัวผู้ป่วย (VMAT) โดยที่วัดรังสี OSL ชนิด OSL และ OSLN เพื่อวัดรังสีในหุ่นจำลอง Alderson Rando โดยใช้แผนการรักษาที่ได้จากการผู้ป่วยมะเร็งต่อมลูกหมาก ทำการเปรียบเทียบปริมาณรังสีโฟตอนกระเจิงและนิวตรอนที่ได้จากการฉายรังสีทั้ง 3 เทคนิค ที่ผิวของหุ่นจำลองด้านนอกของลำรังสีโฟตอนและที่อวัยวะสำคัญ พบว่าปริมาณรังสีสมมูลโฟตอนกระเจิงและนิวตรอนสูงสุดเมื่อใช้เทคนิคการฉายรังสีแบบปรับคงความเข้ม รังสีสมมูลนิวตรอนเฉลี่ยที่บริเวณท้องเท่ากับ 0.26, 0.63 และ 0.31 mSv/Gy ซึ่งเป็นระยะทางห่างจากจุดหมุนของเครื่องฉายรังสี 20 ซม. ขณะที่ปริมาณรังสีสมมูลโฟตอนกระเจิงเท่ากับ 6.94, 10.17 และ 6.56 mSv/Gy โดยใช้เทคนิคการฉายแบบ 3 มิติ แบบปรับความเข้มและแบบปรับความเข้มหมุนรอบตัวผู้ป่วยตามลำดับ การวัดปริมาณรังสีสมมูลใน 7 อวัยวะพบว่าปริมาณรังสีสมมูลสูงสุดเมื่อใช้เทคนิคการฉายแบบปรับความเข้ม ปริมาณรังสีสมมูลที่ตับ ซึ่งเป็นอวัยวะที่ใกล้จุดศูนย์กลางการหมุนของเครื่องที่สุด ได้รับปริมาณรังสีสมมูลโฟตอนกระเจิงและนิวตรอนเท่ากับ 10.23 และ 0.73 mSv/Gy ผลการศึกษาพบว่าปริมาณรังสีสมมูลมากที่สุด เมื่อใช้เทคนิคการฉายรังสีแบบปรับความเข้ม ปริมาณรังสีสมมูลที่ได้จากการฉายรังสีแบบปรับความเข้มหมุนรอบตัวผู้ป่วยมีปริมาณรังสีใกล้เคียงกับเทคนิคการฉายรังสี 3 มิติ ดังนั้นการเลือกเทคนิคการฉายรังสีที่เหมาะสมสามารถช่วยลดปริมาณรังสีที่ไม่พึงประสงค์แก่ผู้ป่วยและเจ้าหน้าที่ปฏิบัติงานได้

ภาควิชา	วิศวกรรมนิวเคลียร์	ลายมือชื่อนิสิต	
สาขาวิชา	วิศวกรรมนิวเคลียร์	ลายมือชื่อ อ.ที่ปรึกษาหลัก	
ปีการศึกษา	2557	ลายมือชื่อ อ.ที่ปรึกษาร่วม	

The scatter photons and neutrons from high energy photon beams (more than 10 MV) will increase the undesired dose to the patient and the staff working in linear accelerator room. This undesired dose which is found at out-of-field area can increase the probability of secondary malignancy. The purpose of this study is to determine the equivalent dose of scatter photons and neutrons generated by 3 different treatment techniques: 3D-conformal, IMRT and VMAT. The measurement was performed using two types of the Optically Stimulation Luminescence (OSL and OSLN) detectors in the Alderson Rando phantom that was irradiated by 3 different treatment techniques following the actual prostate cancer treatment plans. The scatter photon and neutron equivalent dose were compared among the 3 treatments techniques at the surface in the out-of-field area and the critical organs. Maximum equivalent dose of scatter photons and neutrons was found when using the IMRT technique. The neutrons showed average equivalent doses of 0.26, 0.63 and 0.31 mSv/Gy at abdominal surface region which was 20 cm from isocenter for 3D, IMRT and VMAT, respectively. The scattered photons equivalent doses were 6.94, 10.17 and 6.56 mSv/Gy for 3D, IMRT and VMAT, respectively. For the 7 organ dose measurements, the scattered neutron and photon equivalent doses in out of field from the IMRT plan were highest. At the liver which was the nearest organ at out of field, the average equivalent dose were 0.73, 10.23 mSv/Gy for neutron and photon, respectively. The result revealed that the scatter equivalent doses for neutron and photon were higher for IMRT. The equivalent doses for VMAT were slightly higher than 3D. So the suitable treatment techniques should be selected to benefit the patient and the treatment room staff.

Department:	Nuclear Engineering	Student's Signature	....
Field of Study:	Nuclear Engineering	Advisor's Signature	....
Academic Year:	2014	Co-Advisor's Signature	....

ACKNOWLEDGEMENTS

CONTENTS

Page

LIST OF TABLES

LIST OF FIGURES

LIST OF ABBREVIATION

ABBREVIATION	TERM
2D	Two Dimension
3D-CRT	Three Dimensional Conformal Radiation Therapy
AAA	Anisotropic Analytical Algorithm
BNCT	Boron Neutron Captured Therapy
CT	Computed Tomography
Gy	Gray
ICRP	*International Commission on Radiological Protection*
IMRT	Intensity Modulated Radiation Therapy
keV	Kilo Electron Volt
LED	Light Emitting Diode
LINAC	Linear Accelerator
MC	Monte Carlo Simulation
MeV	Mega Electron Volt
MLC	Multileaf Collimator
mSv	Milli Sievert
MU	Monitor Unit
MV	Mega Voltage
OSL	Optically stimulated luminescence
PMT	Photomultiplier Tube
RT	Radiation Therapy
SSD	Source Skin Distance
TLD	Thermoluminescent Detector

CHAPTER 1

INTRODUCTION

1.1 Background and Rational

In external beam radiation therapy, a combination of megavoltage photon beam and radiation treatment technique is commonly employed to eradicate tumor cells in a cancer patient. The beam can be generated using a linear accelerator (LINAC), and the beam energy is selected based upon various considerations, including the type of cancers and the treatment technique to utilize. For instance, the 6 MV photon beam is used for brain, head and neck regions, whereas the high energy photon beam of greater than 10 MV is used for deep tumors in the pelvic area such as prostate cancer. The higher energy beam provides many advantages over the lower energy one such as deeper penetration for higher depth dose, reducing skin dose, and decreasing peripheral dose due to smaller scatter. In the clinical work, these advantages must be quantified and accounted into the calculation of patient's dose distribution in order to get an accurate dose value.

Nevertheless when the photon energy is sufficiently high, e.g. greater than 10 MV, unwanted neutrons can also be produced through the photoneutron (γ,n) interaction.[1] The photon energy required for the interaction must be sufficient, i.e. 5-15 MeV[2], to offset the binding energy of the nucleons in the high-atomic-number (high-Z) materials that compose the LINAC head components such as the target, primary collimators, flattening filter, secondary collimator, and MLCs. The produced neutrons can go on to activate nearby materials, or leave the LINAC head into the treatment room. During the treatment, the employed orientation and field size of the collimator jaws and the MLCs can also vary the amount of neutrons produced. These neutrons can cause the increase in the total

dose received by the patient as well as the staff who access the treatment room immediately after the treatment, contributing to the future risk of secondary malignancy in the patient and the additional occupational exposure of the staff.

In the past decade, the intensity modulated radiation therapy (IMRT) treatment technique has been utilized for treating many types of cancer instead of the conventional 3D-conformal treatment technique. IMRT can reduce dose in critical organ since the isodose coverage can be adjusted to match the shape of the tumor. Another new technique that has been gaining popularity in recent years is the volumetric modulated arc therapy (VMAT) treatment technique. In VMAT, the dose is delivered to the whole volume rather than slice-by-slice. It employs the treatment planning algorithm to ensure the treatment precision, which helps minimize the dose to surrounding healthy tissue. The VMAT consumes less treatment time than IMRT with the same prescription dose.

The IMRT technique is widely used for prostate cancer treatment. It deploys higher monitor unit (MU) than the 3D-conformal technique for the same prescription dose. Therefore, more scatter photons and neutrons are produced inside the treatment room which leads to higher undesired dose to the patient and staff. This secondary dose of scatter photons and photoneutrons can increase the risk of malignancy. Followill et al estimated the x-ray and neutron leakage for high energy photon beam of 6, 18 and 25 MV to be 190, 911 and 1686 mSv in total prescription dose of 70 Gy at isocenter, respectively.[3] The increased risk of secondary cancer due to the leakage is in the range of 1.00% for 6 MV to 24.4% for 25 MV. Reft et al used TLDs to measure the neutron equivalent dose at the out-of-field of the 18 MV photon beam.[4] The results revealed that the IMRT neutron equivalent dose normalized to the prescription dose varied from 2 to 6 mSv/Gy. Kry et al have also estimated the out-of-field photon and neutron equivalent dose from the step-and-shoot IMRT technique, the neutron equivalent dose to each critical organ, and the risk of malignancies.[5]Neutrons equivalent

dose to each organ was found to be within the 2.5-9.0 μSv/MU range when the photon treatment energy was 15 MV.

The photoneutrons in radiotherapy machine were studied under various aspects.[6-12] Their characteristics were determined based on different analytical techniques that inconsistently revealed large variations of neutron equivalent dose. There were two contributions to these variations. First, the studies used different instrumentations and methods of calculation for the photoneutron dose. Second, the neutron equivalent dose depended on the components of the LINAC head, the environment of the treatment room, and the energy of the photon beam.

Most studies also reported the neutron dose produced from the 18 MV photon beam which was higher than the photon energy of our concern. Only few reports investigated the neutron equivalent dose produced by the 15 MV photon beam. Howell et al measured the neutron spectrum using the gold foil activation in Bonner spheres.[6] The average neutron energy was found to be 0.23 MeV for the 15 MV photon beam utilized in the Varian LINAC machine. Zabihzadehet et al studied the neutron equivalent dose and the neutron spectra using the Monte Carlo (MC) simulation based upon a simple model of the LINAC head.[7] The neutron equivalent dose was found to be 4.1 mSv/Gy for the 15 MV photon beam. Due to the simplicity of the model used in the study, the accuracy of the MC calculation was expected to be compromised.

For measurement, most studies used the TLD to determine the neutron equivalent dose. Nedaie et al used TLD-600/TLD-700 dosimeters to measure the neutron equivalent dose and compared with the result from Monte Carlo simulation.[8] Other passive detectors such as gold foil, CR-39 track etch detectors, and bubble detectors are also commonly used for this purpose. Neutrons can induce the nuclei in gold foil to emit radiation that can be measured by the Ge(Li) detector system. The intensity of neutron flux can be estimated from the level of the induced radioactivity. The CR-39 detector measurement is based on counting the number of ionization tracks etched into the surface of the

CR-39 detector after irradiation. Neutrons cannot generate any ionization track in the detector directly. However, neutrons can produce charge particles such as proton and alpha that can in turn cause ionization. For instance, the recoil protons can be produced by the interactions between the neutrons and the hydrogen atoms contained in a polyethylene radiator, and the alpha particles can be produced from the $^{10}B(n,\alpha)^7Li$ reactions in a boron loaded radiator. These charge particles can produce tracks on the detector, and the dose can then be evaluated by counting the number of tracks.

The bubble detector consists of tiny droplets of superheated liquid that disperses throughout a clear polymer. After the neutron strikes a droplet, the droplet immediately vaporizes, forming visible gas bubble trapped in the gel. The number of bubbles yields direct measurement of the neutron tissue-equivalent dose. Fujibuchi et al measured the secondary neutron dose for the 10 MV and the 15 MV X-ray LINACs using the gold foil and the CR-39 detectors.[13]The results showed that the neutron dose from the 15 MV LINAC was 10 times higher than the dose from the 10 MV LINAC because the cross-section of the photonuclear reaction increased.

Viamonte et al showed that the Optically Stimulation Luminescence (OSL) system was also suitable for the dosimetry related measurement of high-energy photon beams.[14] The results showed good agreement with the ionization chamber and the diode measurements at similar positions. Yukihara et al investigated the OSL detectors produced by Landauer.[15] The reproducibility of the OSL signal for multiple irradiations was found to be on the order of 1%. OSL dosimeter is therefore proven to be suitable for dosimetry measurement in radiotherapy. However, there has been no report so far of using OSL to measure the neutron equivalent dose in medical LINAC with a 15 MV x-ray beam.

Inside the treatment room, not only neutrons are generated. Gamma rays are also generated as the result of interactions between the photoneutron and the high-Z materials in the LINAC head or the treatment room through the (n,γ)-type

reaction. Since the gamma rays can be emitted around the treatment room, it undesirably increases the dose to the patient and the staff who access the treatment room during and shortly after the treatment. Rawlinson et al and Fischer et al reported detection of many activation products, which varied in type, quantity, and location, from different LINAC machines and room geometries.[16, 17] The total annual dose that radiation therapist received during routine work were in the range of 0.7-5 mSv per year.[18-20]

The gamma spectrum of the induced radioactivity should be further investigated in order to identify the types and quantities of the isotopes involved. The excess dose should be quantified in order to correctly implement radiation protection policy in the treatment room, i.e. the occupancy dose should not exceed the dose limit prescribed in the ICRP103 document.[21] This research is to investigate the neutron spectra and dose equivalent around the LINAC head at various distances, as well as the effect of using different field sizes for the treatment. The MC simulation has been employed to estimate the photoneutron spectra in the LINAC machine. The simulation has been setup to match the machine's geometry and position in an actual treatment room at King Chulalongkorn Memorial Hospital. The spectrum of photoneutron has been investigated at the target, collimator, and isocenter of machine. The neutron dose obtained from the simulation has also been compared with the actual measurement using OSL. The activation product and gamma dose are investigated inside the treatment room by measurement. Then, this work is aimed to estimate the scatter photon and neutron equivalent dose from 15 MV photon beams used 3D, IMRT and VMAT treatments in the out-of-field and the in-field areas. The equivalent doses were measured in each critical organ using the Optically Stimulation Luminescence (OSL) detectors.

1.2 Research Objectives

      1. To investigate the neutron spectra and dose equivalent at various distances from isocenter, varied SSD as well as the effect of using different field sizes for the treatment.

      2. To estimate the scatter photon and neutron equivalent surface doses and organ doses from 15 MV photon beams for 3D, IMRT and VMAT treatments in the out-of-field and the in-field areas

CHAPTER 2
LITERATURE REVIEWS

2.1 Theories

2.1.1 Radiation-induced secondary cancer

There are several different mechanisms of radiation carcinogenesis after radiation therapy (RT). They become critical at different dose levels, and in different organs and age groups. The mechanisms are due in large part to the killing or malfunction of cells, and are characterized by a threshold dose. The ICRP called them deterministic. On the other hand, at low doses the mechanisms which may become critical are those so-called stochastic.[21] In this case, the appearance of gene or chromosomal mutations due to the induction of DNA strands may lead to cancer.

Exposure to ionizing radiation is known to increase the future incidence of cancer, particularly leukemia. The mechanism by which this occurs is well understood, but quantitative models predicting the level of risk remain controversial. The most widely accepted model posits that the incidence of cancers due to ionizing radiation increases linearly with effective radiation dose at a rate of 5.5% per sievert.[21]

The linear dose-response model suggests that any increase in dose, no matter how small, results in an incremental increase in risk. The linear no-threshold model (LNT) hypothesis is accepted by the International Commission on Radiological Protection (ICRP) and regulators around the world. According to this model, about 1% of the global population develop cancer as a result of natural background radiation at some point in their lifetime.[22] The equation for calculating risk of secondary cancer are shown in table 2.1

Table 2.1 The equation for calculating risk of secondary cancer.

Calculation	Equation
Linear no-threshold	$F(D)=\alpha\cdot D$
Linear quadratic	$F(D)=\alpha\cdot D+\beta\cdot D^2$
Hormesis	$F(D)=\alpha\cdot[D-\beta]$

where

F(*D*) is the fraction of cells surviving a dose *D*;

α is a constant describing the initial slope of the cell survival curve;

β is a smaller constant describing the quadratic component of cell killing.

In all three cases, the values of alpha and beta must be determined by regression from human exposure data. Laboratory experiments on animals and tissue samples is of limited value. Most of the high quality human data available is from high dose individuals, above 0.1 Sv, so any use of the models at low doses is an extrapolation that might be under-conservative or over-conservative. There is not enough human data available to settle decisively which of these model might be most accurate at low doses. The consensus has been to assume linear no-threshold because it the simplest and most conservative of the three.

The latency period needed for secondary cancer development is difficult to determine because it is the late effect (long time effect). Given that some currently employed RT techniques still lead to a large volume outside the treatment area receiving low dose, evaluation of the dose received over the whole

body of patient (even in the distant region) will provide valuable information for the future epidemiologic studies.

Harmful effects from irradiating healthy tissue can include fibrosis, sterility, and the induction of secondary malignancies, particularly in the breast, thyroid, and lung. The induction of fatal secondary malignancies is considered the greatest risk associated with secondary radiation from radiation therapy.[23] The probability of fatal secondary cancer is shown in table 2.2.

Table 2.2 The probability of fatal secondary cancer in each organ.

Organ	Probability of fatal cancer (%/Sv)
Bladder	0.30
Bone marrow	0.50
Bone surface	0.05
Breast	0.20
Esophagus	0.30
Colon	0.85
Liver	0.15
Lung	0.85
Ovary	0.10
Skin	0.02
Stomach	1.10
Thyroid	0.08
Remainder of body	0.50
Total	5.00

2.1.2 Peripheral dose

A peripheral dose is defined as the dose outside a treatment field. In radiotherapy, the peripheral dose was specifically defined as the dose measured beyond 5 cm from the irradiated volume. For the clinical photon beam, the peripheral dose is produced by the secondary photons that originate by means of LINAC head leakage, scattering at the beam collimator and the flattening filter (head scatter), and scattering from the directly irradiated region on the patient or phantom (internal scatter). While the head scatter can be avoided by adjusting the beam collimator and the flattening filter in the LINAC head, the internal scatter is largely unavoidable. For a high energy photon beam, e.g. greater than 10 MV, the interactions between the photons and the materials inside the LINAC head can also lead to the production of neutrons.

2.1.3 Neutron Production

In a medical LINAC, electrons and photons are the particles intended to cause desired therapeutic effect against cancer cells. When these particles impinge on surrounding materials in the LINAC head, the electrons may undergo electroneutron $(e, e'n)$ interactions that provide the electron energy more than 10 MeV[24] and the photons may undergo photoneutron (γ,n) interactions that occur in the high energy photon beam of greater than 10 MV.[1] Neutron is emitted from the interaction between photon and the nuclei of a high-atomic-number (high-Z) material when the photon energy is higher than the binding energy (5-15 MeV) of the nucleons.[2] The LINAC head components, including the target, primary collimators, flattening filter, secondary collimator, and MLCs (Fig.2.1), are usually made of high Z materials such as W, Pb, Fe, and Cu. Thus, the undesired neutrons can be produced and leave the accelerator head into the treatment room.
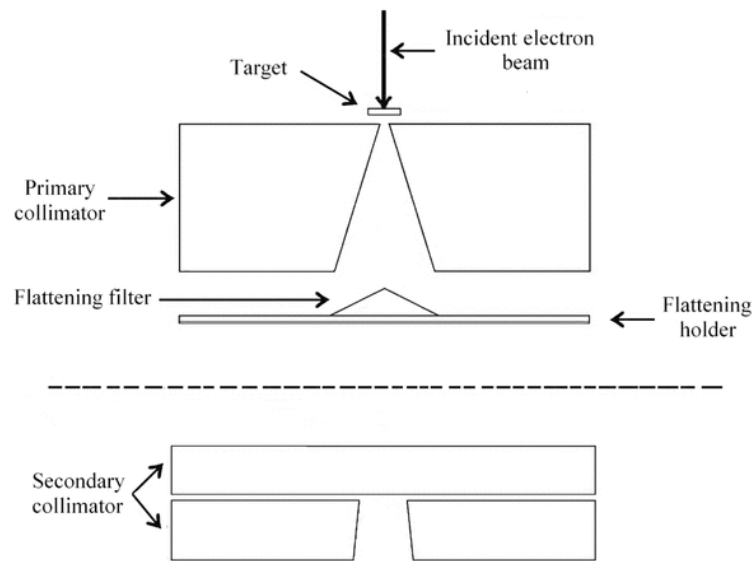
Fig.2.1 Sketch of head components capable of photo-neutron production.

The photoneutron production process is governed by the neutron separation energy and the photoneutron cross-section. The neutron separation energy is the threshold energy that must be overcome in order for the interaction to occur. In the case of the direct effect, a photon interacts with the neutron in a nucleus, and transfers its energy to the neutron. This causes the neutron to be knocked out of the nucleus.

Several nucleons can be emitted through photonuclear reactions, but most common at the energies used in radiotherapy is the emission of a single neutron. In order to calculate the required energy for the photon to kick out a neutron from the nucleus, the neutron separation energy, $Sn(Z, N)$ can be estimated. This is given by

$$Sn(Z, N) = B(Z, N) - B(Z, N - 1) \qquad (2.1)$$

where B is the binding energy of the nucleus

$$B(Z, N) = \left(Z \times m_{(1H)} + N \times m_n - m(Z, N) \right) 931.5 \, MeV \quad (2.2)$$

$m_{(1H)}$ is the mass of a hydrogen atom and m_n is the neutron mass. Because high-Z materials like lead or tungsten are used as collimators for photon beams, the probability for lead nuclei photon interactions is quite large.

When a photo-neutron interaction takes place, one or more neutrons may be σ produced. Therefore the photo-neutron production cross-section is the sum of α(γ,1n), α(γ,2n), α(γ,3n) and so on, where α(γ,1n) usually contributes most. The parameter for photoneutron interaction can be summarized as follow:

1. The energy dependence of $\sigma_\gamma\,(E)$ is dominated by the "gigantic resonance" which can be described by the following lorenzian equation.

$$\sigma_\gamma\,(E) = \frac{\sigma_0}{(1+\frac{(E^2-E_0)}{E_\gamma^2 \cdot \Gamma^2})^2}$$

(2.3)

where

σₒ is the value of the resonance cross section.

Eo is the resonance energy, and

Γ is the resonance width.

2. Above the (y, n) reaction threshold, the increase of the neutron width quickly overwhelms the competing radiative decay; as a result, the contribution of this channel can be neglected.

3. For energies above Eo, on the right side of the gigantic resonance the cross section can noticeably exceed the lorenzian extrapolation, sometimes by a factor of two. There is a tendency to consider this to be a contribution of resonances of other multipolarities, primarily quadripolarity. If one approximates this contribution by alorenzian as well, then its characteristics are most probably the following:

(I)   the resonance energy is larger than the dipolar resonance by 10-15 MeV,

(II) its amplitude is one order of magnitude lower, and

(III) its width is approximately the same

In the photonuclear process, high-energy electron beam interacts on a target material, and continuous spectrum of bremsstrahlung photons is produced. These bremsstrahlung photons subsequently interact with the nucleus of the target material, resulting in the emission of the nucleons. This interaction is known as photonuclear interaction. The absorption of a photon leads to the formation of a compound nucleus which decays by the emission of one or more neutrons. In order for the neutron to be produced, the absorbed photon must have energy greater than the binding energy of the neutron to the nucleus. This threshold depends on the atomic number of the target. For high atomic numbers it is around 8 MeV while for even-even nuclides with low atomic numbers, the threshold is higher (16 MeV for oxygen, 18 MeV for carbon). This neutron flux could find application in industrial and medical fields such as boron neutron captured therapy (BNCT) and neutron radiography. Therefore LINACs with photon energies in the range of 18–25 MeV can produce undesired fast neutrons. During cancer treatment with medical linear accelerator, neutrons might be produced in the accelerator head, typically collimators, target and flattening filter, and even the patient's body.

As the nucleons are bounded with the nucleus by binding energy (5-15 MeV), the photon should have energy above a threshold value to participate in the photonuclear reaction. Neutrons from the photon induced giant-dipole-resonance (GDR) reaction consist of a large portion of evaporation neutrons which dominate at low neutron energies (< 1-2 MeV), and a small fraction of direct neutrons, which dominate at high energies [6]. The photoneutron energy spectrum is characterized by an evaporation peak in the range 200–700 keV and

a relatively weak (10% of the integrated intensity) direct-reaction component in the several MeV energy range.

Neutron can be classified as follows:

Thermal
- Neutrons in thermal equilibrium with their surroundings
- Most probable energy at 20 degrees (C) - 0.025 eV;

Epithermal
- Neutrons of energy greater than thermal
- Greater than 0.2 eV

Cadmium
- Neutrons which are strongly absorbed by cadmium
- Less than 0.4 eV

Epicadmium
- Neutrons which are not strongly absorbed by cadmium
- Greater than 0.6 eV

Slow
- Neutrons of energy slightly greater than thermal
- Less than 1 to 10 eV (sometimes up to 1 keV)

Resonance
- In pile neutron physics, usually refers to neutrons which are strongly captured in the resonance of U-238, and of a few commonly used detectors (e.g., Indium, Gold, etc.)
- 1 eV to 300 eV

Intermediate
- Neutrons that are between slow and fast
- Few hundred eV to 0.5 MeV

Fast
- Greater than 0.5 MeV

Ultrafast

- Relativistic
- Greater than 20 MeV

Pile

- Neutrons of all energies present in nuclear reactors
- 0.001 eV to 15 MeV

Fission

- Neutrons formed during fission
- 100 keV to 15 MeV (Most probable: 0.8 MeV; Average: 2.0 MeV)

2.1.4 Neutron activation

Neutron activation is the process in which a <u>neutron radiation</u> induces <u>radioactivity</u> in a material. It occurs when the <u>atomic nuclei</u> captures <u>free neutron(s)</u>, becoming heavier, and entering <u>excited states</u>. The excited nucleus often decays immediately by emitting <u>gamma ray</u>, or particle such as <u>beta particle</u>, <u>alpha particle</u>, <u>fission product</u> and neutron (in case of <u>nuclear fission</u>). The process of <u>neutron capture</u>, even after any intermediate decay, often results in the formation of an unstable <u>activation product or radioactive nuclei</u>. Such nuclei can exhibit half-life ranging from small fractions of a second to many years. The material is made radioactive (or activated) by the <u>neutron activation process</u>.

Since neutrons have no charge, they only interact with the nucleus of an atom not the electrons. The most common type of neutron induced reaction is the neutron capture reaction (see figure 1 below). When a neutron fuses with the nucleus, a compound nucleus forms in an excited state. The excited compound nucleus will very quickly decay to a more stable state through emission of one or more gamma rays (also known as prompt gamma rays). The new state of the

compound nucleus yields a radioactive nucleus, which will beta decay into an excited state of another radioactive nucleus, which will then decay by emission of one or more gamma rays (also known as characteristic delayed gamma rays). The emission rate depends on the half-life of each radioactive nucleus. The half-life of radioactive nuclei can range from nanoseconds to billions of years.
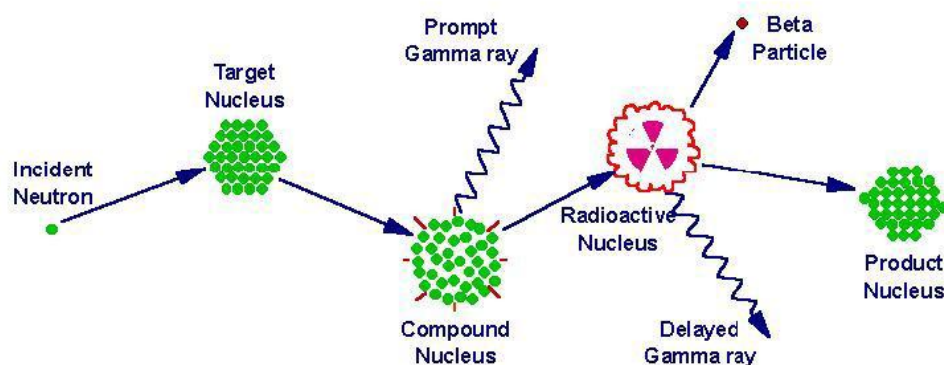
Figure 2.2 Neutron capture reaction.

The activation of a material as a function of time depends upon the material being activated and the beam activating the material. The activity buildup consists of both production and decay terms and may be written as

$$A = N\sigma\phi \left[1 - e^{(-\lambda t_{irrad})}\right] e^{(-\lambda t_{decay})} \tag{2.5}$$

where

    A = activity of the sample as a function of time

    N = number of atoms in the sample that are activated N = m$\bar{\text{A}}$/GAW

    m = mass of the sample (If multiple isotopes are activated, the mass of each constituent must be considered)

    $\bar{\text{A}} = 6.023 \times 10^{23}$ atoms/GAW (Avogadro's number)

    σ = cross section for the reaction induced by the flux Ø (barns/atom)

    Ø = fluence rate or flux (neutrons/cm^2-sec)

    λ = decay constant of the activated material

    GAW = gram atomic weight or mass of a mole of material

t_{irrad}= time the sample was irradiated or exposed to the flux

t_{decay}= decay time or time the sample was removed from the flux

For material that is activated for a long time relative to its half-life, the activity reaches a constant value or saturates. Saturation occurs as the irradiation time becomes much larger than the decay half-life, and the decay time is short relative to the decay half-life. Under these circumstances, the activity approaches A_{sat}, which is the saturation activity

$$A_{sat} = N\sigma\phi \qquad (2.6)$$

Determining the saturation activity is an important exercise because it represents a bounding case for dose rate assessments. The saturation activity ensures that the design will abide any operating condition. Many common activation gamma sources involve the absorption of a neutron with the emission of a gamma ray. Usually this process involves thermal neutrons. Other reactions involve high-energy or fast neutrons and produce high-LET protons via (n, p) reactions. Examples of activation sources are contained in table 2.3. These sources are frequently produced in reactor or accelerator environments.

Table 2.3 Activation gamma sources.

Reaction	Activation Cross Section (barns)	Half-life	Energy (MeV)	Yield Gammas/decay
^{23}Na(n, y)^{24}Na	0.534	14.96 hr	1.369	1.00
			2.354	1.00
^{54}Fe(n, p)^{54}Mn	1.00	314 days	0.835	1.00
^{55}Mn(n,y)^{56}Mn	13.3	2.576 hr	0.847	0.99
			1.811	0.29
			2.11	0.15
^{59}Co(n, y)^{60}Co	37.2	5.263 years	1.173	1.00
			1.332	1.00
^{58}Fe(n, y)^{59}Fe	1.2	45.6 days	1.095	0.56
			1.292	0.44
^{94}Zr(n,y)^{95}Zr	0.075	65.5 days	0.724	0.49
			0.756	0.49
			0.765	1.00

2.1.5 Neutron interaction types

A neutron can have many types of interactions with a nucleus as shown in figure 2.3. Each category of interaction in the figure consists of all those linked below it. The total cross section σ_T expresses the probability of any interaction taking place.

An interaction may be one of two major types scattering or absorption. When a neutron is scattered by a nucleus, its speed and direction change but the nucleus is left with the same number of protons and neutrons it had before the

interaction. The nucleus will have some recoil velocity and it may be left in an excited state that will lead to the even release of radiation. When a neutron is absorbed by a nucleus, a wide range of radiations can be emitted or fission can be induced.

```
                         ┌──────────┐
                         │  TOTAL   │
                         └────┬─────┘
              ┌───────────────┴───────────────┐
        ┌───────────┐                   ┌────────────┐
        │ SCATTERING│                   │ ABSORPTION │
        └─────┬─────┘                   └──────┬─────┘
```

ELASTIC	INELASTIC	ELECTRO-MAGNETIC	CHARGED	NEUTRAL	FISSION
(n,n)	(n,n')	(n,γ)	(n,p) (n,α) (n,d) etc.	$(n,2n)$ $(n,3n)$ $(n,4n)$ etc.	(n,f)
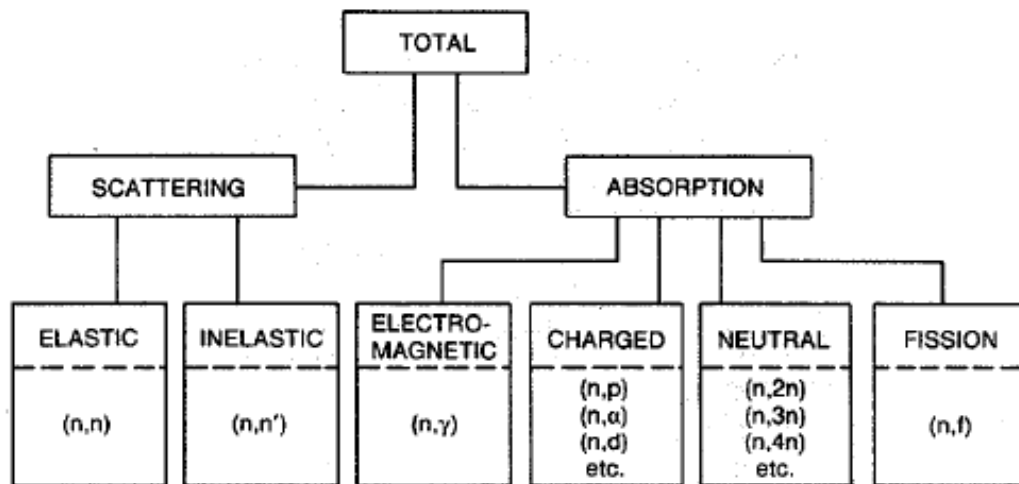
Figure 2.3. Types of neutron interaction.

The neutron may be absorbed or captured. A variety of emissions may follow, as shown in figure 2.3. The nucleus may rearrange its internal structure and release one or more gamma rays. Charged particles may also be emitted the more common ones are protons, deuterons, and alpha particles. The nucleus may also rid itself of excess neutrons. The emission of only one neutron is indistinguishable from a scattering event. This is a cause of activation products inside the treatment room that depends on the neutron energies, materials of LINAC component and types of neutron cross section.

2.1.6 Optically stimulated luminescence (OSL)

An optically stimulated luminescence (OSL) is a detector for ionizing radiation dosimetry. It makes use of <u>electrons</u> trapped between the valence and conduction bands in the <u>crystalline</u> structure of a material (such as <u>quartz</u>, <u>feldspar</u>, and <u>aluminium oxide</u>). The trapping sites are imperfections of the lattice-impurities or <u>defects</u>. The ionizing radiation produces electron-hole pairs in which the electrons are in the <u>conduction band</u> and the holes are in the <u>valence band</u>. The electrons which have been excited to the conduction band may become entrapped in the electron or hole traps. Under stimulation of light, the electrons may free themselves from the trap and get into the conduction band. From the conduction band, they may recombine with holes trapped in hole traps. If the center with the hole is a luminescence center (radiative recombination center), emission of light will occur. The <u>photons</u> are detected using a <u>photomultiplier</u> tube. The signal from the tube is then used to calculate the dose that the material had absorbed.

The OSL dosimeter provides a new degree of sensitivity by giving an accurate reading as low as 1 mrem for x-ray and gamma ray photons with energies ranging from 5 keV to greater than 40 MeV. The OSL dosimeter's maximum equivalent dose measurement for x-ray and gamma ray photons is 1000 rem. For beta particles with energies from 150 keV to in excess of 10 MeV, dose measurement ranges from 10 mrem to 1000 rem. Neutron radiation with energies of 40 keV to greater than 35 MeV has a dose measurement range from 20 mrem to 25 rem.

The N-Type Optically Stimulation Luminescence (OSLN) used in this study consists of the single crystal carbon doped aluminum oxide (Al_2O_3:C). OSL technology is the newest advancement in passive radiation dosimetry. The read out process uses a light emitting diode (LED) array to stimulate the detector. The light emitted from the OSL detector is then measured by a photomultiplier tube (PMT) counting system (Inlight system, Landauer). The OSLN dosimeter is capable of measuring neutron energies between 40 to 5000 keV. The OSLN contains Al_2O_3:C

coated with $^6Li_2CO_3$. Neutron interacts with ^6Li and produces both tritium and alpha particles following equation 2.7. These particles give up their energy to the Al_2O_3:C in a process that generate a stored charge. OSLN detectors can be annealed to remove existing measurement using the Landauer's model 50A automatic annealer. So, OSLN can be repeatedly used for measuring neutron dose.

$$Li^6 + n_0^1 \xrightarrow{yields} He^4(2.05\ MeV) + H^3(2.75\ MeV) \qquad (2.7)$$
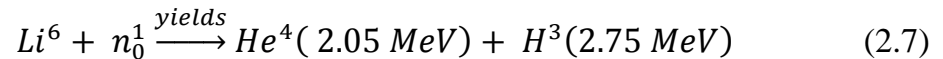
For mixed beam irradiation, OSL dosimeters were used to measure the photon only, while OSLN dosimeters were used to measure both photon and neutron. The neutron dose was determined by subtracting the photon signal measured by OSL dosimeters from the signal measured by the OSLN dosimeters. Both types of OSL should be used at the same time for measurement.

2.1.6.1 Characteristics of OSL for radiotherapy applications[25]

OSL has many characteristics that are suitable for radiotherapy applications, including

- Small size
- Good reproducibility
- None or well defined environmental corrections
- Dose linearity
- Dose rate independence
- Energy independence
- No directional dependence -isotropic response to radiation

2.1.6.2 Advantages and disadvantages of OSL

The advantage and disadvantage of OSL are shown in table 2.4.

Table 2.4 The advantage and disadvantage of OSL

Advantages	Disadvantages
• High sensitivity	• Sensitivity to light
• High precision	• Non-tissue equivalent – energy
• Size	dependence
• Convenience	
• Readout flexibility	
• Fast non-destructive readout	
dependence	
• No significant fading – dose storage	
• No need for annealing	

2.1.7 Monte Carlo simulation

2.1.7.1 History

Monte Carlo is well suited to solving complicated three-dimensional, time-dependent problems. Because the Monte Carlo method does not use phase space boxes, there are no averaging approximations required in space, energy, and time. This is especially important in allowing detailed representation of all aspects of physical data. The neutrons of concern have a wide energy range, the use of detector may lead to large uncertainty in the measurement of the neutron dose. Many methods for dose estimation have been taken into consideration, and the Monte Carlo (MC) simulation which is often used in radiation transport modeling is found to be one of the most powerful methods for the estimation of neutron dose. In MC simulation, the interactions of particles within a material follow a certain probability distribution which is represented by random numbers. The tracks of each particle are recorded (history) and used to calculate the dosimetric quantities.

Most types of neutron interactions and their conditions are taken into account in the MC simulation. Assuming that the geometry and material compositions have been accurately modeled, the simulation can closely represents all the interactions that occur in the real situation. Hence, the neutron dose can be predicted and investigated.

2.1.7.2 MCNP code

MCNP is a general-purpose Monte Carlo N–Particle code. It can calculate for neutron, photon, electron, or coupled neutron/photon/electron transport, including the capability to calculate eigenvalues for critical systems. The code arranges an arbitrary three-dimensional configuration of materials in geometric cells bounded by first- and second-degree surfaces and fourth-degree elliptical tori. Important standard features that make MCNP very versatile and easy to use include a powerful general source, criticality source, and surface source; both geometry and output tally plotters; a rich collection of variance reduction techniques; a flexible tally structure; and an extensive collection of cross-section data.

MCNP is a general-purpose, continuous-energy, generalized-geometry, time-dependent, coupled neutron/photon/electron Monte Carlo transport code. It can be employed in several transport modes: neutron only, photon only, electron only, combined neutron/photon transport where the photons are produced by neutron interactions, neutron/photon/electron, photon/electron, or electron/ photon.

A standard feature, the user can create an input file that is subsequently read by MCNP. This file contains information about the problem in areas such as the geometry specification, the description of materials and selection of cross-section evaluations, the location and characteristics of the neutron, photon, or electron source, the type of answers or tallies desired, and any variance reduction techniques used to improve efficiency.

MCNP can be used to duplicate theoretically a statistical process (such as the interaction of nuclear particles with materials) and is particularly useful for complex problems that cannot be modeled by computer codes that use deterministic methods. The individual probabilistic events that comprise a process are simulated sequentially. The probability distributions governing these events are statistically sampled to describe the total phenomenon. In general, the simulation is performed on a digital computer because the number of trials necessary to adequately describe the phenomenon is usually quite large. The statistical sampling process is based on the selection of random numbers. It consists of actually following each of many particles from a source throughout its life to its death in some terminal category (absorption, escape, etc.). Probability distributions are randomly sampled using transport data to determine the outcome at each step of its life that is shown in figure 2.4. This neutron history is now complete. As more and more such histories are followed, the neutron and photon distributions become better known. The quantities of interest (whatever the user requests) are tallied, along with estimates of the statistical precision (uncertainty) of the results.

Event Log

1. Neutron scatter, photon production
2. Fission, photon production
3. Neutron capture
4. Neutron leakage
5. Photon scatter
6. Photon leakage
7. Photon capture
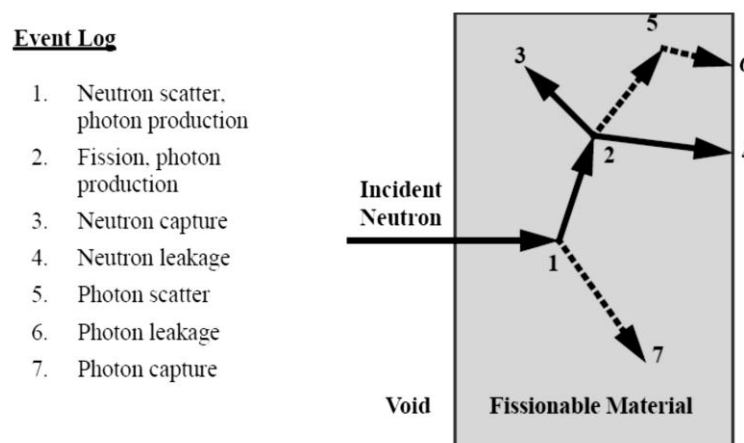
Figure 2.4. The random history of a neutron incident on a slab of material.

2.1.7.3 MCNP process

MCNP is written in ANSI-Standard Fortran 90.22 Global data is shared via Fortran modules. The Monte Carlo transport workhorse, MCNP [Los Alamos National Laboratory report LA-13709-M, 2000], is undergoing a massive renovation at Los Alamos National Laboratory (LANL) in support of the Eolus Project of the Advanced Simulation and Computing (ASCI) Program. MCNP Version 5 (V5) (expected to be released to RSICC in Fall 2002) will consist of a major restructuring from FORTRAN-77 (with extensions) to ANSI-standard FORTRAN-90 [American National Standard for Programming Language – Fortran-Extended, ANSI X3. 198-1992, 1992] with support for all of the features available in the present release (MCNP-4C2/4C3).

This capability has been reviewed, slightly modified, and incorporated into MCNP Version 5 for neutron and photon applications. The method uses multiple point detectors to determine the particle flux at pixel locations in a user-defined grid. As many detector points as desired can be used to create both the direct (unscattered) and scattered flux image contributions. Each source and collision event contributes to all detectors, resulting in a smooth image.

The general internal structure of MCNP is as follows:

Initiation (IMCN):

• Read input file (INP) to get dimensions;

• Set up variable dimensions or dynamically allocated storage;

• Re-read input file (INP) to load input;

• Process source;

• Process tallies;

• Process materials specifications including masses without loading the data files;

• Calculate cell volumes and surface areas.

Interactive Geometry Plot (PLOT).

Cross-section Processing (XACT):

• Load libraries;

Plot tallies, cross sections, and other data (MCPLOT).

The MCNP code package is incomplete without the associated nuclear data tables in libraries. The kinds of tables available and their general features are outlined in this section. The manner in which information contained on nuclear data tables is used in MCNP

Nine classes of data tables exist for MCNP libraries. They are: (1) continuous-energy neutron interaction data; (2) discrete reaction neutron interaction data; (3) continuous-energy photoatomic interaction data; (4) continuous-energy photonuclear interaction data; (5) neutron dosimetry cross sections; (6) neutron $S(\alpha,\beta)$ thermal data; (7) multigroup neutron, coupled neutron/photon, and charged particles masquerading as neutrons; (8) multigroup photon; and (9) electron interaction data.

2.1.7.4 MCNP geometry

The geometry of MCNP treats an arbitrary 3-dimensional configuration of user-defined materials in geometric cells bounded by first- and second-degree surfaces and fourth-degree elliptical tori. The cells are defined by the intersections, unions, and complements of the regions bounded by the surfaces. Surfaces are defined by supplying coefficients to the analytic surface equations or, for certain types of surfaces, known points on the surfaces. MCNP also provides a "macrobody" capability, where basic shapes such as spheres, boxes, cylinders, etc., may be combined using boolean operators.

MCNP manages geometric cells in a Cartesian coordinate system that it used is arbitrary and user defined.

2.1.7.5 Tallies and output

MCNP can make various tallies related to particle current, particle flux, and energy deposition. MCNP tallies are normalized to be per starting particle except for a few special cases with criticality sources. Currents can be tallied as a function of direction across any set of surfaces, surface segments, or sum of surfaces in the problem. Charge can be tallied for electrons and positrons. Fluxes across any set of surfaces, surface segments, sum of surfaces, and in cells, cell segments, or sum of cells are also available. Similarly, the fluxes at designated detectors (points or rings) are standard tallies, as well as radiography detector tallies. Fluxes can also be tallied on a mesh superimposed on the problem geometry. Heating and fission tallies give the energy deposition in specified cells. A pulse height tally provides the energy distribution of pulses created in a detector by radiation. In addition, particles may be flagged when they cross specified surfaces or enter designated cells, and the contributions of these flagged particles to the tallies are listed separately. Tallies such as the number of fissions, the number of absorptions, the total helium production, or any product of the flux times the approximately 100 standard ENDF reactions plus several nonstandard ones may be calculated with any of the MCNP tallies. In fact, any quantity of the form

$$C = \int \emptyset(E)f(E)dE \qquad (2.8)$$

can be tallied, where $\phi(E)$ is the energy-dependent fluence, and *f(E)* is any product or summation of the quantities in the cross-section libraries or a response function provided by the user.

All tally results, can be displayed graphically, either while the code is running or in a separate post processing mode.

2.1.8 Equivalent dose and effective dose

2.1.8.1 Equivalent dose

The equivalent absorbed radiation dose, usually shortened to equivalent dose, is a computed average measurement of the radiation absorbed by a fixed mass of biological tissue that attempts to account for the different biological damage potential of different types of ionizing radiation. It is therefore a less fundamental quantity than the total radiation energy absorbed per mass (the absorbed dose), but is a more significant quantity for assessing the health risk of radiation exposure.

It is adequate for assessing risk due to external radiation fields that penetrate uniformly through the whole body, but needs further corrections when the field is applied only to part of the body or when it is due to an internal source. A further quantity called effective dose can be calculated if the fractionation of radiation to different parts of the body is known, to take into account the varying sensitivity of different organs to radiation. Another quantity called committed dose is used when the radiation source has entered the body.

Equivalent dose is dimensionally a quantity of energy per unit of mass, and is measured in Sieverts or rems. The equivalent dose is calculated by multiplying the absorbed dose, averaged by mass over an organ or tissue of interest, by a radiation weighting factor appropriate to the type and energy of radiation. To obtain the equivalent dose for a mix of radiation types and energies, a sum is taken over all types of radiation energy dose as follows:

$$H_T = W_R \; x \; D_{T,R} \qquad\qquad (2.8)$$

where

H_T is the equivalent dose absorbed by tissue T (Sv),

$D_{T,R}$ is the absorbed dose in tissue T by radiation type R (Gy), and

W_R is the radiation weighting factor defined by regulation and is given in Table 2.5.

Table 2.5 Radiation weighting factors W_R (formerly termed Q factor) used to represent <u>relative biological effectiveness</u> according to ICRP report 103.[21]

Radiation	Energy	W_R (formerly Q)
X-rays, Gamma rays, Beta rays, Muons		1
Neutrons	< 1 MeV	$2.5 + 18.2 \cdot e^{-[\ln(E)]^2/6}$
	1 MeV - 50 MeV	$5.0 + 17.0 \cdot e^{-[\ln(2 \cdot E)]^2/6}$
	> 50 MeV	$2.5 + 3.25 \cdot e^{-[\ln(0.04 \cdot E)]^2/6}$
Protons, Charged pions		2
Alpha rays, Nuclear fission products, Heavy nuclei		20

2.1.8.2 Effective dose

The effective dose in radiation protection and radiology is a measure of the cancer risk to a whole organism due to ionizing radiation delivered non-uniformly to parts of body. It takes into account both the type of radiation and the nature of each organ being irradiated. The effective dose is not intended as a measure of deterministic or other effects of radiation although it is used to estimate inherited effects.

The effective dose replaces the former effective dose equivalent, and is sometimes incorrectly called the dose equivalent, but should not be confused with the equivalent dose. Equivalent dose does not consider the type and amount of tissue exposed, so an equivalent dose applied to only a portion of the body will carry lower risk than if the same equivalent dose was applied to the whole body. An effective dose will carry the same effective risk to the whole organism regardless of where it was applied, and it will carry the same effective risk as the same amount of equivalent dose applied uniformly to the whole body. These doses can be added together and hence assume a linear no threshold model of cancer risk.

The unit for effective dose is the sievert (Sv), or the rem, the same as for equivalent dose. One Sievert equals one joule/kilogram(J/kg).

The US Nuclear Regulatory Commission still endorses the ICRP's 1977 tissue weighting factors in their regulations, in spite of the ICRP's later revised recommendations.

The effective dose of radiation (E) is found by calculating a weighted average of the underlined equivalent dose (H_T) in different body tissues, with the weighting factors (W_T) designed to reflect the different importance of tissue types to the danger to the whole organism. Where the dose is only applied to a portion of a tissue or organ, it needs to be averaged across the entire mass of the tissue or organ in order to be representative of that tissue type.

$$E = H_T \times W_T \tag{2.9}$$

Where

E is the effective dose to the entire organism (Gy)

H_T is the equivalent dose absorbed by tissue T (Sv)

W_T is the tissue weighting factor defined by regulation and is given in table 2.6

Table 2.6 Tissue weighting factors W_T for different organs.

Organs	Tissue weighting factors		
	ICRP26 1977	ICRP60 1990	ICRP103 2007
Gonads	0.25	0.20	0.08
Red Bone Marrow	0.12	0.12	0.12
Colon	-	0.12	0.12
Lung	0.12	0.12	0.12
Stomach	-	0.12	0.12
Breasts	0.15	0.05	0.12
Bladder	-	0.05	0.04
Liver	-	0.05	0.04
esophagus	-	0.05	0.04
Thyroid	0.03	0.05	0.04
Skin	-	0.01	0.01
Bone surface	0.03	0.01	0.01
Salivary glands	-	-	0.01
Brain	-	-	0.01
Remainder of body	0.30	0.05	0.12
Total	1.00	1.00	1.00

2.1.9 Radiation treatment techniques

Radiotherapy is one of the main methods of the cancer treatment. The radiation treatment technique has been evolved from the two dimensional radiotherapy (2D), three dimensional conformal radiotherapy (3D-CRT) to the intensity modulated radiotherapy (IMRT), and the latest volumetric modulated arc therapy (VMAT).[26] The 2D technique uses 2D image from a conventional simulator for dose calculation. This technique is suitable for a conventional treatment that typically uses single or two-parallel opposing fields. The 3D-CRT is based on the CT image for dose calculation. The use of forward planning with suitable beam parameters are selected by planner to get the confirm dose to target volume and minimize radiation dose to critical organs. The 3D treatment planning is shown in figure 2.4

The IMRT technique is the inverse planning technique for dose calculation. It uses the multi-leaf collimator (MLC) to modulate the radiation beam intensity, and relies on a 3D image calculation to compute the suitable variation of intensity patterns in each treatment field. Hence, the radiation dose will conform to the tumor shape, and spare dose to normal organs when combining all the fields together. The dose constraints are defined for the planning target volume (PTV) and the normal organs to optimize the dose. The IMRT treatment consumes higher monitor unit (MU) as compared to the 3D-CRT treatment with the same treatment time. The IMRT planning is shown in figure 2.5

VMAT is the newest radiation treatment technique which is more complicated than the IMRT technique. It not only modulates the beam with the MLC motion, but also varies the dose rate and gantry speed during treatment. VMAT can improve the dose conformity and coverage to the target volume, and spare the dose to normal organs. VMAT consumes lower MU than IMRT, which can help reduce the treatment time. The VMAT treatment planning is shown in figure 2.6. The treatment planning procedures of 3D-CRT, IMRT and VMAT are shown in figure 2.7
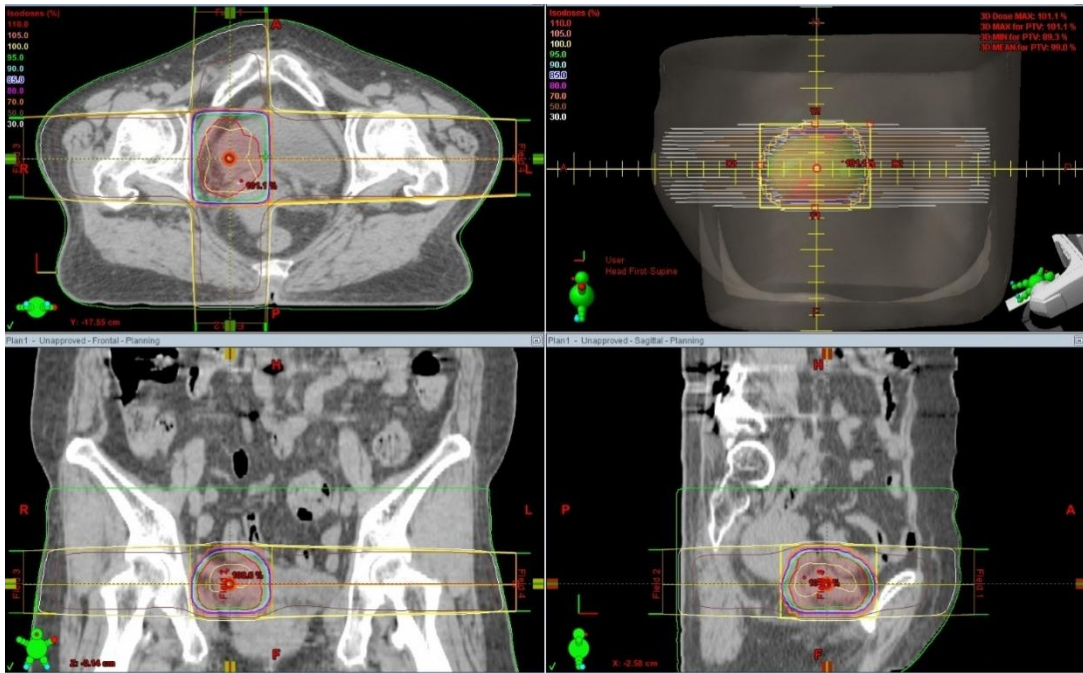
Figure 2.5 The 3D planning for 4 fields.
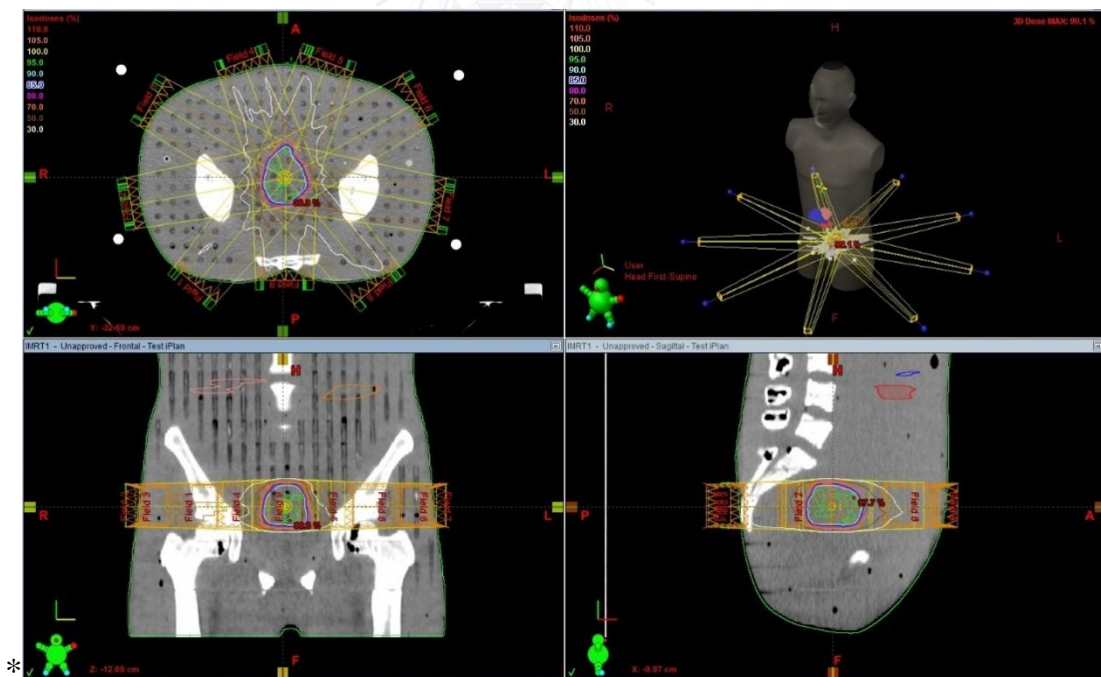
Figure 2.6 The IMRT planning for 9 fields.
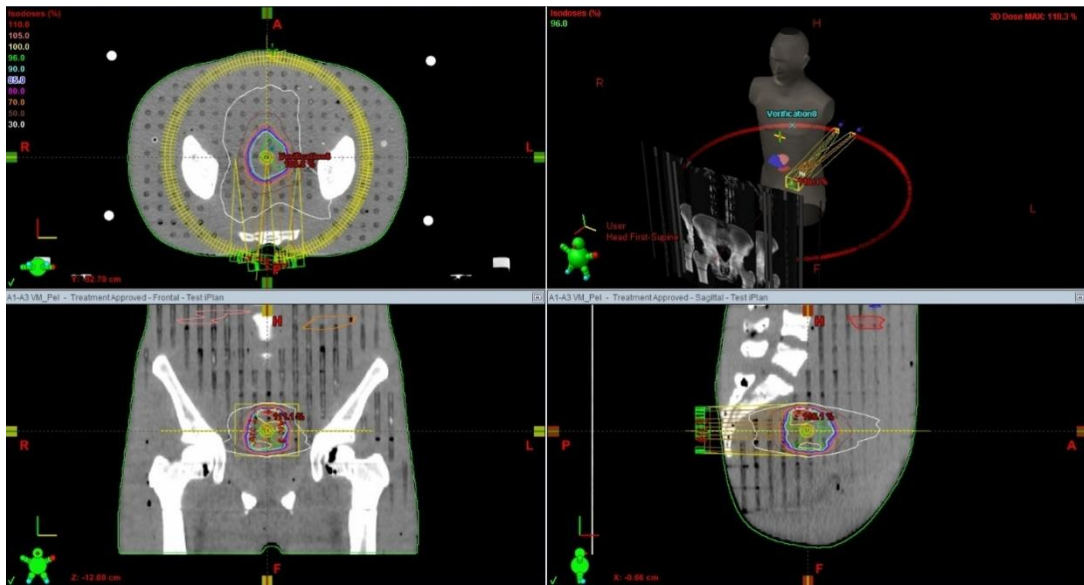
Figure 2.7 The VMAT planning for 2 Arcs rotation.
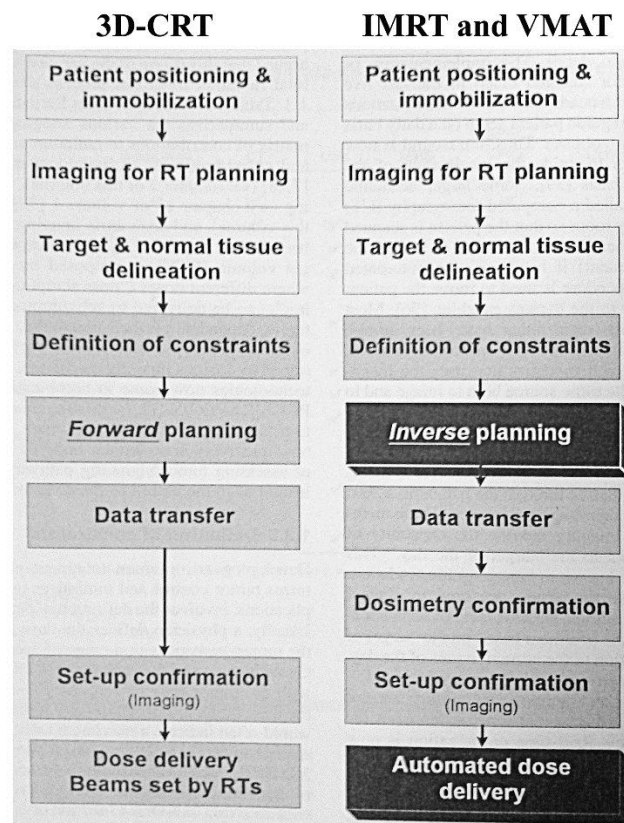
Figure 2.8 Comparison of the procedure of the radiation treatment planning and dose delivery for the 3D-CRT, IMRT and VMAT techniques.

2.1.9.1 Forward planning

Forward planning is a technique used in <u>external-beam radiotherapy</u> to produce a treatment plan. In forward planning, a treatment uses beams into a radiotherapy <u>treatment planning</u> system which can deliver sufficient radiation to a <u>tumor</u> while both sparing critical <u>organs</u> and minimizing the dose to healthy tissue. The required decisions include how many radiation beams to use, which angles each will be delivered from, whether attenuating <u>wedges</u> be used, and which <u>multileaf collimator</u> (MLC) configuration will be used to shape the radiation from each beam.

Once the treatment planner has made an initial plan, the treatment planning system calculates the required monitor units to deliver a prescribed dose to a specific area in the patient which is dependent on beam modifiers that include wedges, specialized collimation, field sizes, tumor depth, etc. The information from a prior <u>CT scan</u> of the patient allows more accurate modeling of the behavior of the radiation as it travels through the patient's tissues. Different dose prediction models are available, including <u>pencil beam</u>, <u>convolution-superposition</u> and <u>Monte Carlo simulation</u>, with precision versus computation time being the relevant trade-off.

2.1.9.1 Inverse planning

For inverse planning, a desired dose distribution is defined (by the definition of constraints), and the computer calculates the required beam intensities and shapes to beast meet the specified dose distribution or treatment objectives. With inverse planning, the user does not directly optimize or readjust beam intensities. If the optimized plan is not considered acceptable, then the planner has to modify the dose-volume constraints and restart the optimization process.

Central to the inverse planning algorithm is an objective function (a mathematical function that describes the quality of a treatment plan. Various mathematical procedures have been developed to minimize the objective

function, usually by going through some type of iterative process. Objective functions can be based on dose criteria, dose-volume criteria, or biological criteria.

2.2 Review of Related Literatures

Many researchers studied the neutron dosimetry for high energy beam in radiotherapy. They compared doses obtained from measurement and calculation, and reported the comparisons as follows.

Howell et al[27] measured the secondary neutron equivalent dose from conventional and intensity modulated radiation therapy (IMRT) prostate treatments for 15 and 18 MV x-ray beams. Both techniques used the prescription dose of 45 Gy to the prostate. The neutron dosimeter was the TLD-based system. The treatments using 18 MV IMRT and conventional plans resulted in the neutron ambient equivalent dose of 687 and 112 mSv, respectively. For 15 MV, the IMRT and conventional plans resulted in the neutron ambient equivalent dose of 327 and 52 mSv, respectively. The results showed the advantage of using lower photon energies for IMRT to reduce the secondary neutron dose, while still achieving comparable treatment volume coverage and sparing critical normal tissues.

Kry et al[28] focused on neutrons that were produced by high energy radiation therapy and a source of dose to normal organ. Thus, the presence of neutrons increased the patient's risk of radiation-induced secondary cancer. In the study, the authors characterized properties of neutrons produced by the high energy photon beams (18 MV) at different depths inside the patient for different field sizes and source-to-surface distances (SSD). They used a previously developed Monte Carlo model of an accelerator operated at 18 MV to calculate the neutron fluence, energy spectra, quality factors, and equivalent dose in air and in tissue at the depth range from 0.1 to 25 cm. The results showed that the neutron fluence decreased as the depth increased. The average neutron energy

decreased sharply with increasing depth up to 7.5 cm depth in tissue, and remained nearly constant afterward. The neutron equivalent dose increased slightly with increasing field size and decreasing SSD. When the neutron equivalent dose is determined inside the patient, the spectrum and quality factor used should be adjusted to reflect the depth instead of using the in-air conditions.

Howell et al[29] studied effective dose from the delivery of 6 MV, 15 MV, and 18 MV conventional and intensity modulated radiation therapy (IMRT) prostate treatment plans. Neutron spectra were measured for 15 MV and 18 MV. ICRP-74 quality conversion factors were used to calculate equivalent dose. The IMRT treatments resulted in an overall decrease in the effective dose compared to the conventional treatments. In comparison among the three beam energies used for the IMRT treatments, 6 MV resulted in the lowest effective dose, while 18 MV resulted in the highest effective dose. This was attributed to the large neutron contribution in the 18 MV beam as compared to no neutron contribution in 6 MV beam.

Relt et al[4] provided in vivo patient and phantom measurements of the secondary out-of-field photon radiation and the neutron equivalent dose for the 18 MV IMRT treatments using difference treatment machines and treatment planning systems. The secondary photon and neutron equivalent doses were compared between the IMRT plan and the six-field three-dimensional conformal radiotherapy (3D-CRT) plan. For in vivo measurements, the thermoluminescent detectors (TLDs) and the Al_2O_3 detectors employing optically stimulated radiation were used to obtain the photon equivalent dose; and the CR-39 track etch detectors were used to obtain the neutron equivalent dose. For phantom measurements, a Bonner sphere containing two types of TLDs (TLD-600 and TLD-700) having different thermal neutron sensitivities were used to obtain the out-of-field neutron equivalent dose. The results for the 18 MV IMRT plan showed that the photon equivalent dose was greater than the neutron equivalent dose measured outside the treatment field. The neutron equivalent dose

normalized to the prescription dose varied from 2 to 6 mSv/Gy depending on the treatment machine.

Aoyama et al[30] studied neutron dose to radiotherapy patients treated with 10 MV x-ray beams based on the spectrometry of incident photoneutrons. The neutron energy spectra were obtained by unfolding measured responses of neutron capture rates of indium activation foils in a polyethylene phantom with response functions calculated by Monte Carlo simulation. Unfolded neutron spectra inside and outside the x-ray beam indicated that photoneutrons distributed in the energy region of less than 1 MeV with the maximum fluence per unit lethargy at around 0.1 MeV. Effective dose to the patient was adopted as a fundamental protection quantity since photoneutrons from the accelerator head were found to enter the whole body of the patient with approximately flat intensity. Outside the X-ray beam, the dose was evaluated to be 59 μSv/photonGy by using the neutron energy fluence to the effective dose conversion-coefficients for calculating neutron dose which was tabulated by the ICRP for anterior-posterior irradiation geometry. Since the total effective dose received by the patient during the treatment period, which corresponded to an integral photon dose of 60 Gy, was estimated to be as small as 3.5 mSv, no additional shield would be required for contaminant photoneutrons generated by the 10 MV therapeutic x-rays.

CHAPTER 3
RESEARCH METHODOLOGY

This study is divided into 3 parts:

1. Neutron spectrum and neutron dose estimation.
2. Activation products and gamma equivalent dose investigation.
3. Scatter photon and neutron equivalent dose in vivo dosimetry.

The high energy photon beams (15 MV) are used to treat the patient. It can create the unwanted doses inside the treatment room. The unwanted doses are divided into 3 types: neutron doses, scatter photon doses, and gamma doses.

Neutron doses are produced by high energy photon interaction with high Z materials. The neutron can subsequently activate activation produces, leading to emission of gamma ray inside the treatment room. The scatter photons, which are secondary photons from the primary photon beam, can hit any material and change their direction.

Neutron doses are of concern for both patient and radiotherapist -- the scatter photon doses to the patient, and the gamma doses to the radiotherapist. These unwanted doses increase the risk of secondary cancer.

3.1 Neutron spectrum and neutron dose estimation

The neutron spectrum was estimated by Monte Carlo simulation to investigate the neutron energy produced inside the treatment room. The neutron energy was used for the neutron dose calculation in another Monte Carlo simulation, which converted the neutron flux to neutron dose. In addition, the neutron energy was also used for computing the equivalent dose of neutron with the radiation weighting factor (W_r). The use of the Monte Carlo simulation was due to the difficulty in directly measuring the neutron energy by a detector. The neutron energy spectrum could be alternatively found by simulation. The energy

spectrum was then employed to calculate the neutron equivalent dose in subsequent part of the study

The neutron equivalent dose was assessed by two approaches: simulation with the Monte Carlo method and measurement by the OSL. The neutron equivalent dose at various distances from isocenter, at different SSD, as well as the effect of using different field sizes for the treatment was studied. This experiment is explained in chapter 4.

3.2 products and gamma equivalent dose investigation.

The high energy photon can cause productions of neutrons inside the LINAC head. The neutrons can subsequently activate the LINAC materials to radionuclide that emits gamma ray. Many radionuclides can be induced inside treatment head. So, the activation products and gamma equivalent dose should be investigated for the purpose of radiation protection in terms of the types of produced radionuclides and the gamma spectrum. The gamma doses were investigated around the gantry of LINAC. The gamma doses represented the dose-to-staff in term of mSv/h. The result revealed the gamma dose that the radiotherapist might obtain while working in the treatment room. This experiment is explained in chapter 5.

3.2 Scatter photon and neutron equivalent dose in vivo dosimetry.

The scatter photon and neutron equivalent doses were measured by the OSL to estimate the surface equivalent doses, the equivalent doses in organ, and the effective doses from 15 MV photon beams for 3D, IMRT and VMAT treatments in the out-of-field and the in-field areas. For the surface equivalent doses, the OSL was used to measure the dose at the head, neck, chest, abdomen and pelvis regions. For the critical organ dose, the OSL was used to measure the equivalent dose in the brain, thyroid, lung, stomach, liver, bladder and rectum. The OSL and OSLN were placed on the Rando phantom to measure the equivalent doses.

Then, the equivalent doses were compared among the 3 treatment techniques. The equivalent doses were subsequently used for the effective dose calculation. This experiment is explained in chapter 6.

CHAPTER 4
NEUTRON DOSE EQUIVALENT ESTIMATION

4.1 Materials and Methods

4.1.1. Monte Carlo calculation

The Monte Carlo simulation in this study is based on the MCNP code version 5 (MCNP5), and has been customized for the calculations of neutron spectrum and neutron equivalent dose. Several components of the LINAC head, including the target, primary collimator, flattening filter, secondary collimator and MLCs, were simulated based on the 15 MV photon beam source CLINAC 23EX machine (Varian Medical Systems, Palo Alto, CA, USA), shown in figure 4.1. The geometrical data of each component were obtained from the manufacturer and used as the input for the MCNP5 code. The head of LINAC created by the MCNP is shown in figure 4.2. All geometrical data can be found in Appendix A.
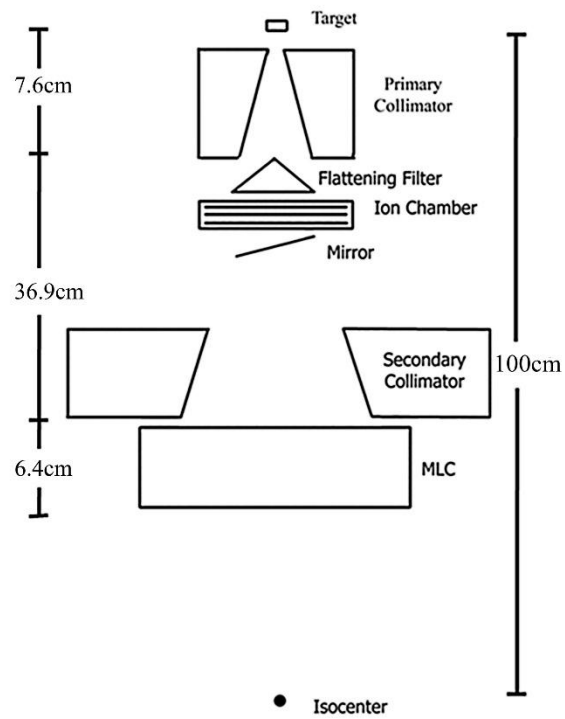
Figure 4.1 Sketch of head components of Varian CLINAC 23EX for simulation.
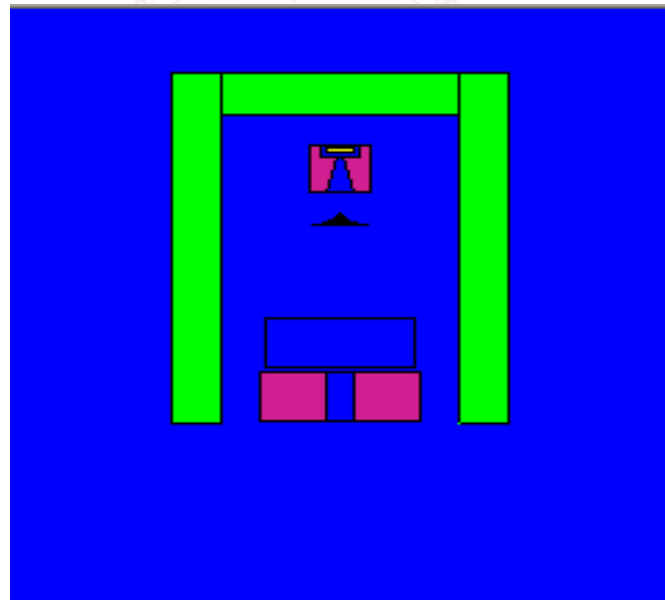
Figure 4.2 The head of LINAC created by MCNP.

A 15 MV photon beam in Gaussian energy distribution mode was used as a primary source. The energy cutoff was set at 0.1 MeV to reduce the calculation time for photon because the photon energy must be higher than 10 MeV in order to produce photoneutron. The incident electron energy was adjusted in the MCNP code until the percentage depth dose (PDD) and the beam profile matched the beam data measured by ionization chamber (0.13cc volume) within 1% as shown in figure 4.3. The PDD and beam profile were compared in the 10×10 cm^2 of 15 MV photon beam. The final incident electron energy used in the simulation was 13.5 MeV. The neutron spectrum and flux were calculated using 10^7 simulate particles. The photon-electron-neutron transport mode was used for running the simulation. The simulated detection volume had a cylindrical shape with 1-cm radius and 1-cm thickness. The human body was modeled with a water equivalent phantom sized $30 \times 30 \times 30$ cm^3. The neutron flux was also computed in the F4 tally mode, and was converted to the neutron equivalent dose using the flux-to-dose conversion factor from the ICRP 74. The calculation uncertainty in each energy bin was less than 3%. The MCNP5 code was set to determine the neutron spectrum and average neutron energy. The neutron spectrum was simulated at the target, collimator, and isocenter of the beam. The neutron dose at each position of measurement was compared with the OSL measurement.
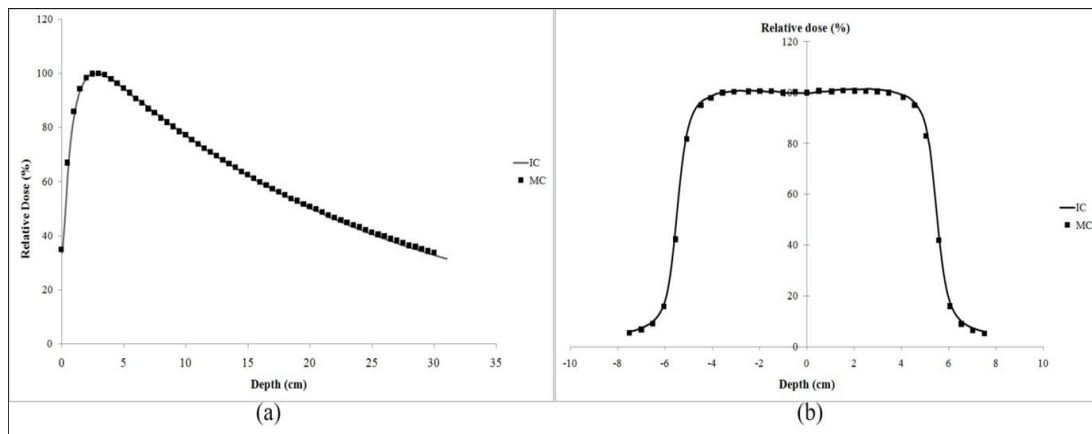
Figure 4.3 Percentage depth dose curve and beam profile of 15 MV x-rays compared between Monte Carlo simulation and ionization chamber. (a) PDD opening 10x10 cm^2 field size. (b) Beam profile opening 10x10 cm^2 at 10 cm depth.

4.1.2. Optically Stimulation Luminescence (OSL) measurement

The OSL detectors were placed on a solid water phantom at various positions for measurement during the delivery of the 15 MV photon beam. For mixed beam irradiation, the OSL dosimeters were used to measure the photon only, while the OSLN dosimeters were used to measure both the photon and neutron. The neutron dose was determined by subtracting the photon signal measured by OSL dosimeters from the photon-neutron signal measured by the OSLN dosimeters. Both types of the OSL should be used at the same time for measurement. The nanoDot type of OSL which was employed for this study is shown in figure 4.4. The maximum relative sensitivity of the OSL varied about 3.1% of one standard deviation.[25] At each position, the measurement was repeated 5 times, and the average reading in the unit of mSv per photon Gy was reported. The OSL detectors were calibrated with ^{137}Cs gamma source and the OSLN detectors were calibrated with ^{252}Cf neutron source because the energy range of ^{252}Cf covered the energy range of the photoneutrons generated inside the treatment head of the LINAC.

4.1.3. Neutron dose equivalent comparison

The neutron equivalent doses in the unit of mSv per photon Gray (mSv/Gy) obtained from simulation and measurement were compared under various conditions. In this study, several combinations of collimator jaw's field size, SSD, off-axis distance, and MLC's field size shown in table 4.1 have been investigated. The monitor units were 1000 MU used to expose on the OSL in each measurement. These MUs represented the IMRT treatment. The measurements of OSL set up in each position were shown in figure 4.5

Figure 4.4 The OSL nanoDot type.

Table 4.1 The various parameters for simulation and measurement.

Experiment	Field size (cm²)	SSD (cm)	Off axis distance (cm)	Field Size by MLC (cm²)
1	2x2 5x5 10x10 15x15 30x30	100	0	N/A
2	10x10	80 100 150 200	0	N/A
3	10x10	100	0 100 150 200	N/A
4	30x30	100	0	2x2 5x5 10x10 15x15
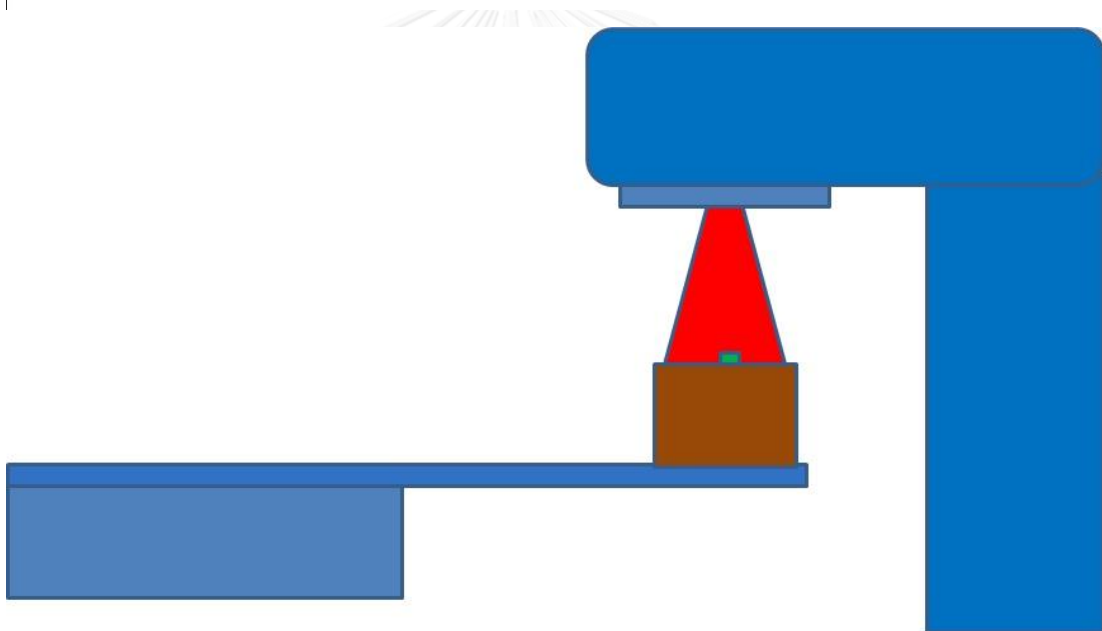
Figure 4.5 The equivalent dose measurement by OSL in each position.

4.2 Results

4.2.1. Neutron Spectra

The neutron spectrum was simulated for the 15 MV photon beam modeled after the Varian 23EX linear accelerator. The number of initial electrons used for the simulation was 10 millions. The components of Linear accelerator head were created according to the data from manufacturer. However, a smaller boundary is used instead of the actual room geometry to reduce the calculation time. The neutron spectra were calculated by the MCNP5 code at the target, collimator jaws, and isocenter of the field, as shown in figure 4.6. The average neutron energy was 0.25 MeV and the maximum energy was 0.49 MeV.
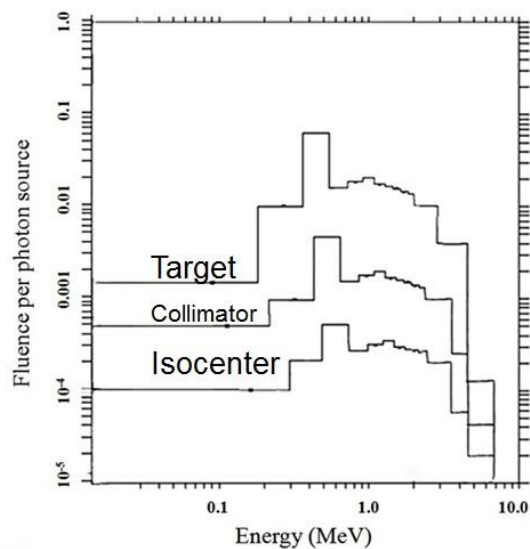
Figure 4.6 Neutron spectra simulated by Monte Carlo Method at the target, the primary collimator and the isocenter positions.

4.2.2. Neutron equivalent dose

Neutrons are generated from the interactions between the high energy photon beam and the components of the linear accelerator that have high atomic number. In this study, the MCNP5 code was used to simulate these interactions, and the results were compared against the actual measurement. In the simulation, the components of the linear accelerator head were modeled according to the manufacturer's specification, and the problem geometry followed the setup of the actual experiment. In the experiment, the neutron equivalent dose was measured with the OSLN at various positions inside the treatment room.

For different field sizes, the measured and calculated neutron equivalent doses are shown in table 4.2. The OSL was irradiated at 100 cm SSD on top of the $30x30x30$ cm^3 solid water phantom. The ranges of the measured and calculated neutron doses for 2x2, 5x5, 10x10, 15x15, and 30x30 cm^2 were 3.79 - 6.75 mSv/Gy and 3.45 - 6.31 mSv/Gy, respectively. All data from the OSL measurements are given in Appendix B.

Table 4.2 Neutron equivalent doses for different field sizes by jaws.

Field size (cm^2)	Measurement	Calculation
	(mSv/Gy)	
2x2	3.79 ± 0.05	3.45
5x5	4.09 ± 0.09	3.79
10x10	5.39 ± 0.05	4.34
15x15	5.61 ± 0.06	4.53
30x30	6.75 ± 0.08	6.31

The neutron equivalent dose was also investigated for different SSDs with the same field size of 10x10 cm^2. The measurement and calculation at different SSD positions yielded the range of neutron doses between 2.41 - 7.45 mSv/Gy and 1.95 - 6.98 mSv/Gy, respectively, as shown in table 3.3. All data from the OSL measurements are given in Appendix C.

Table 4.3 Neutron equivalent doses at different distances.

SSDs (cm)	Measurement	Calculation
	(mSv/Gy)	
80	7.45 ± 0.07	6.98
100	5.34 ± 0.07	4.53
150	4.29 ± 0.07	3.97
200	2.41 ± 0.09	1.95

The neutron equivalent doses at the in-field and out-of-field distances are shown in table 4.4. The measured and calculated neutron doses at the isocenter were 5.39 and 4.34 mSv/Gy, respectively. At 100 cm out-of-field, the measured and calculated neutron doses were 0.42 and 0.75 mSv/Gy, respectively. All data from the OSL measurements are given in Appendix D.

Table 4.4 Neutron equivalent doses at in-field and out-of-field distances.

Distance (cm)	Measurement	Calculation
	(mSv/Gy)	
0 (Isocenter)	5.39 ± 0.07	4.34
100	0.42 ± 0.09	0.75
150	0.21 ± 0.08	0.62
200	0.15 ± 0.05	0.43

The comparison between the measured and calculated neutron equivalent doses was performed for various MLC's field sizes while the collimator jaws' field size was fixed at 30x30 cm^2. The results are shown in table 4.5. The neutron equivalent dose increased by closing (reducing) the MLC's field size. All data of OSL measurement are shown in Appendix E.

Table 4.5 Neutron equivalent dose for different field sizes opened by MLCs.

Field size (cm^2)	Measurement	Calculation
	(mSv/Gy)	
2x2	9.75 ± 0.09	9.25
5x5	7.02 ± 0.07	6.51
10x10	4.99 ± 0.08	4.19
15x15	4.32 ± 0.08	3.84

4.3 Discussion

From the neutron spectra in figure 4.6, the average neutron energy was 0.25 MeV and the maximum energy was 0.49 MeV. The result was consistent with the average neutron energy reported by Howell et al[6] and Zabihzadeh et al[7] which were 0.23 MeV and 0.20 MeV, respectively. The neutron spectra calculated at different components and locations of the LINAC had similar shape, but differed in the neutron flux intensity. The highest intensity was found at the target, and the intensity decreased further away from target.

For fast neutron (> 10 keV), the predominant moderating effect came from inelastic scattering in high atomic number materials located inside the components of the LINAC head. However, this interaction would not occur at energy below the lowest exited state of the material. While it was difficult to estimate the neutron energy loss due to inelastic scattering, the loss was minimal since the energy of neutrons produced in the treatment room was mostly less than the lowest exited state. This was the reason why the energy of neutron remained the same when the neutron passed from the target to the isocenter.

Beam hardening effect of photon also occurred inside the LINAC head, causing slightly increase in average neutron energy at the isocenter. Higher energy photon could produce higher neutron energy. The neutron flux intensity reduced from the target to the isocenter because the number of photoneutrons generated inside the LINAC head at the target was higher than at the other components, and the neutron attenuation varied by distance.

The neutron equivalent dose increased for larger field size as shown in table 4.2. The results agreed with the neutron equivalent dose reported in other studies. Zabihzadeh et al[7] reported the neutron equivalent dose of 4.1 mSv/Gy at the isocenter for the 40x40 cm^2 field size calculated by the Monte Carlo simulation. Chibani et al[1] reported the neutron equivalent dose of 13.3 mSv/Gy for the 10x10 cm^2 field size calculated by the MCNPX code in Varian machine. The neutron equivalent dose was also investigated for different SSDs. The

measurement and calculation are shown in table 4.3. The neutron dose decreased as the SSD increased.

In table 4.4, the neutron dose at the out-of-field was less than at the isocenter by several times because the maximum intensity of the neutron fluence was generated at the target of the LINAC head. Therefore, the neutron fluence was partly absorbed by the shielding components of machine. Zabihzadeh et al[7] reported the neutron equivalent dose of 4.1 mSv/Gy at the isocenter and 0.79 mSv/Gy at the distance of 100 cm out-of-field from the isocenter for the 40x40 cm^2 field size in the 15 MV photon beam. The values agreed well with our study. The comparison between the measured and calculated neutron equivalent doses was performed for various MLC's field sizes, while the collimator jaws' field size was fixed. The neutron equivalent dose increased by closing (reducing) the MLC's field size. When the MLC was closed, more neutrons were generated in the MLC which was made of tungsten. Meo et al[12] reported the neutron yield at each component of the LINAC head, which agreed well with our study.

For comparison between the field size opened by jaws and by MLCs, the neutron doses from the field size opened by MLCs were higher than the doses from the field size opened by jaws with the same field size. The reason was that the distance between the MLC and the detector was closer than the distance between the jaws and the detector. The previous experiment investigated the neutron dose when the SSD was varied. The result showed that the neutron dose decreased further away from the LINAC head.

For the in-field positions, the neutron equivalent doses calculated by the MCNP5 were lower than the corresponding values measured by the OSLN. Neutron could scatter with the floor, wall, and ceiling of the treatment room, as well as with other equipment around the treatment room. In order to limit the calculation time, the MC simulation did not include the geometry of every environmental object inside the treatment room. Thus, the calculated neutron

dose was consistently less than the measured neutron dose at every in-field position.

For the out-of-field positions, the neutron doses calculated by the MCNP5 were higher than measurement because the calculation underestimated the shielding components. The shielding thickness of the LINAC head was not included in the simulation due to the lack of information from the manufacturer.

CHAPTER 5
ACTIVATION PRODUCTS AND GAMMA
EQUIVALENT DOSE INVESTIGATION

5.1 Materials and Methods

Neutron can interact with the materials inside the treatment machine, and produce activation products that emit gamma radiation via the (n,γ) reaction. In this thesis, the activation products have been investigated by gamma spectrometry. A radionuclide identifier system was used to determine the emitting isotopes. The system was portable, and utilized the 3"x3" sodium iodide (NaI) scintillation detector (SAM 940 eagle, Berkeley Nucleonics Corporation, San Rafael, CA, USA) that were shown in figure 5.1. The gamma spectrum was collected at 100 cm SSD after finishing the irradiation at 1000 MU because it represented the IMRT treatment technique, and the gamma dose rate in unit of mSv per hour was measured using a survey meter. The survey meter is Victoreen model 190 with energy compensated Geiger-Mueller (GM) Probe Model 90-12 (CardinalHealth, Dublin, OH, USA). The detector was calibrated by secondary standard laboratory (Department of the Medical Science, Ministry of Public Health, Thailand). The detector was put on top of the treatment couch. The gantry was set at 0 degree angle. The spectrum was measured inside the light field when the collimator jaws were opened to 10x10 cm^2. The 15 MV photon beam was delivered at the dose rate of 400 MU/min, i.e. a clinical dose rate. The gamma spectrum and gamma dose was recorded immediately after the irradiation using the recording time of 5 minutes. The spectrum was analyzed in order to identify the isotopes and the percentage yield of each isotope. The gamma dose rate was also measured immediately after the irradiation. The dose rate measurement was repeated at the same position at 5 minutes, 1 hour, 12 hours and 24 hours after the irradiation in order to investigate and analyze the long-half-life isotopes. The gamma dose rate was studied for the purpose of radiation protection for the staff who work in the treatment room.

Figure 5.1 The spectrometer for gamma spectrum and gamma dose measurement.

5.2 Results

The gamma spectrum measured by a spectrometer revealed the gamma peaks that corresponded to several activation products as shown in figure 5.2. A spectrum analysis was able to identify 4 dominant radioisotopes: ^{28}Al, ^{24}Na, ^{54}Mn and ^{60}Co. ^{28}Al displayed the highest peak on the spectrum. The characteristics of each isotope are shown in table 5.1. The spectrum showed the annihilation peak at 511 keV as a result of the beta plus decay from ^{54}Mn.

The gamma equivalent dose rate of 4.14 µSv/h was measured at 100 cm SSD immediately after irradiation at 1000 MU. The dose came from the all activation products inside the treatment room. The equivalent dose rate decreased to 0.65 µSv/h after 5 minutes of waiting time (after the irradiation). The equivalent dose rate became less than 0.001 µSv/h, or the background dose, after allowing 1 hour decay time.
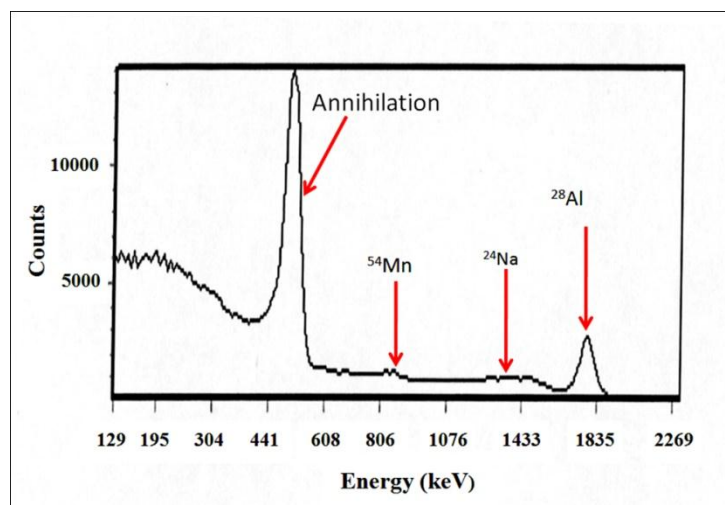
Figure 5.2 Gamma spectrum generated by activation products inside the linear accelerator room.

Table 5.1 The characteristic of activation products generated inside the linear accelerator room.

Nuclides	Gamma energy (keV)	Half life	Dose (μSv/h)	% Yield
^{28}AL	1779	2.24 min	3.565	86.10
^{24}Na	1369	15 h	0.548	13.24
^{54}Mn	847, 1811	2.58 d	0.018	0.43
^{60}Co	1253	5.27 y	0.009	0.20

5.3 Discussion

Several activation products were generated when the photoneutrons interacted with the components of the LINAC head. These activation products emitted gamma ray that might lead to unnecessary exposure of the treatment-room occupancies. Determination of the percentage yield of each radioisotope found that the dominant activation product was ^{28}Al immediately after the irradiation. Several radioisotope products disappeared in a few minutes after the irradiation because of their short half-lives. One hour after the irradiation, ^{54}Mn became the dominant product since most ^{28}Al have decayed; and between 12 and

24 hours following the irradiation, ^{24}Na became the dominant product instead. After 24 hours, the dose rate was nearly at the background level from the contribution of low yield radioisotopes like ^{60}Co and other long half-life radioisotopes. Long half-life radioisotopes have also been reported by Fischer H.W. et al.[17] All of these major radioisotopes were generated by neutron capture interactions because photoneutron interacted with materials inside the treatment head and treatment room.

Since the dominant activation product immediately after the irradiation is ^{28}Al which is a short half-life isotope, protective action against it can be easily taken by the treatment room staff, by allowing the isotope to decay for a short period of time before entering the treatment room after the irradiation. For other isotopes that have longer half-lives, it is found that the personal gamma doses received is about 0.78 mSv/y which is well within the recommended occupational dose limit of 20 mSv/y.[21]

Thus, it is recommended that the therapist or staff should wait for a few minutes before entering the treatment room after irradiation, and stay only for a short period of time. This way, the radiation exposure can be minimized. Before dose measurement in this study, therapist of LINAC 23EX which entered the treatment room immediately received the gamma and neutron dose of 780 μSv/y and 600 μSv/y that the total dose was 1.38 mSv/y. Usually, the therapist of radiotherapy department receives the total dose less than 10 μSv/y that stilled within the dose limited of 20 mSv/y. This dose is safe for radiotherapist.

CHAPTER 6
SCATTER PHOTON AND NEUTRON EQUIVALENT DOSE
IN VIVO DOSIMETRY

6.1 Materials and Methods

6.1.1 Treatment planning

The Eclipse treatment planning software version 11.0.31 (Varian Medical Systems, Palo Alto, CA, USA) was used to calculate dose for the 10 prostate cancer cases selected for this study. The treatments utilized the Varian 23EX linear accelerator (Varian Medical Systems, Palo Alto, CA, USA) with 15 MV photon beams in combination with 3 different treatment techniques. For the VMAT technique, 3 arcs were provided for dose calculation. The IMRT utilized 9 fields (20, 60, 100, 140, 180, 220, 260, 300 and 340 degree) for treatment. The 3D-conformal technique employed 4 fields (0, 90, 180 and 270 degree). The prescribed dose was 2 Gy per fraction for all treatment techniques. The monitor unit (MU) were calculated by using the Anisotropic Analytical *Algorithm (AAA)* for all techniques. All treatment plans were delivered to the Rando phantom in the treatment room. The scatter photon and neutron equivalent doses in various areas were then measured.

6.1.2 Dose Measurement

The Optically Stimulation Luminescence N-type (OSLN) detectors were used for neutron dose measurement in this study. For mixed beam, the OSL measured the photon only, while the OSLN measured both the photon and neutron. Subtraction of the two readings gave the neutron dose. Both types of the OSL were placed together at the defined locations for measurement. The unscreen OSL was employed for this study. The maximum relative sensitivity of the unscreen OSL was about 3.1% of one standard deviation.[25] The OSL and

OSLN were placed on the Alderson Rando phantom (RANDO®Phantoms) surface at the head, cervical, thoracic, abdominal and pelvic regions as shown in figure 6.1. The pelvis region was in the in-field area, while the other regions were in the out-of-field area. The out-of-field region was about 20, 45, 65 and 75 cm away from the isocenter for the abdominal, thoracic, cervical, and head regions, respectively. The OSL and OSLN were put on the left and right sides of the Rando phantom for measurement. The Rando phantom was irradiated by the VMAT, IMRT and 3D techniques, using the actual treatment plans from 10 prostate cancer cases. The measurement was repeated 3 times, and the reading (in the unit of mSv/photon Gy) at each position was averaged. The equivalent doses were compared between the out-of-field and the in-field areas.
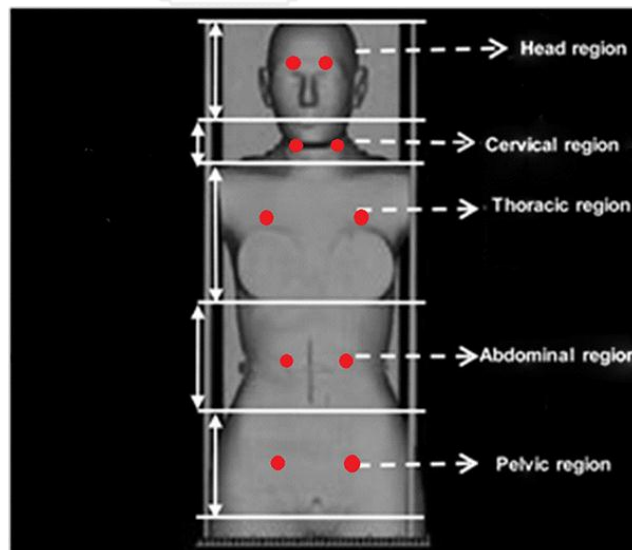
Figure 6.1 Measurement of equivalent surface dose at various regions on Rando Phantom.

The scatter photon and neutron doses in critical organs, such as brain, thyroid, lung, stomach, liver, bladder and rectum, were measured by placing the OSL and OSLN inside each organ inside the Rando phantom. The positions of measurement inside the Rando phantom were shown in figure 6.2. The bladder and rectum were considered within the in-field area for the treatment of prostate cancer. The other organs were considered out-of-field of the treatment area. The Rando phantom was then irradiated by the VMAT, IMRT and 3D techniques planned for the prostate cancer treatment. In each organ, the measurement was repeated 3 times, and its average was reported in term of mSv/photon Gy. The equivalent dose was determined in each organ. The OSL detectors were calibrated with the ^{137}Cs gamma source and the OSLN detectors were calibrated with the ^{252}Cf neutron source. The ^{252}Cf source was selected because, based on the Monte Carlo simulation of photoneutron, the energy range of ^{252}Cf overlapped the energy range of the photoneutrons generated inside the LINAC treatment head. The neutron dose was calculated using the radiation weighting factors which were recommended by the National Council on Radiation Protection and Measurements.[21]
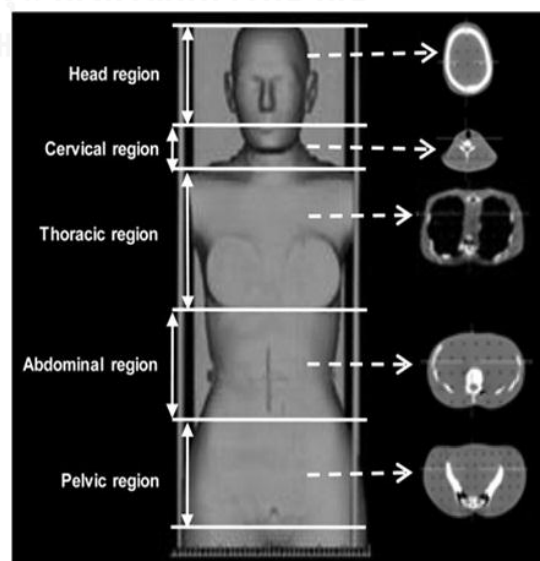
Figure 6.2 Measurement of equivalent dose at various organs inside the slab of Rando Phantom.

The 3D treatment technique used the 4 field in 0, 90, 180 and 270 degree. For IMRT, the 9 fields were used to calculate dose in phantom and the VMAT employed the 3 Arcs for dose calculation around the phantom. The field size varied between 10 to 15 cm in all treatment techniques. The monitor units of each treatment technique employed for one fraction of treatment that was shown in table 6.1.

Table 6.1 The monitor units of the 3D, IMRT and VMAT treatment technique.

Technique	3D	IMRT	VMAT
Num. fields	4 Fields	9 Fields	3 Arcs
MU	250-350	1200-2000	500-850

6.2 Results and discussion

6.2.1. Equivalent surface doses within the in-filed and out-of-field regions.

The average scatter photon and neutron equivalent doses at the head, neck, chest, abdomen regions from 10 prostate cancer cases treated with the 3D, IMRT and VMAT techniques are shown in table 6.2. For the in-field region, i.e. the pelvic region, the average neutron equivalent doses were 1.20, 2.10, and 1.60 mSv/Gy for the 3D, IMRT, and VMAT techniques respectively. The neutron equivalent dose decreased rapidly in the out-of-field region. The dose in the head region was 10 times less than in the pelvic region. The distance between the two positions was 75 cm. Zabihzadeh et al[7] reported the neutron equivalent dose of 4.1 mSv/Gy at the isocenter and 0.79 mSv/Gy at the distance of 100 cm out-of-field from the isocenter for the 40x40 cm^2 field size in the 15 MV photon beam.

In all cases, the neutron doses from the IMRT plan were higher than the doses from the VMAT and the 3D conformal plans. The neutron doses from VMAT plan were slightly higher than the dose from the 3D plan in all regions. The neutron dose depended on the monitor unit (MU) which was highest in the case of IMRT given the same prescribed dose. The IMRT employed the MCLs for adjusting the dose, so the photon can interact and generate the photoneutron to increase the neutron dose more than other techniques. Therefore, the suitable treatment technique can help reducing the neutron dose to out-of-field region of the patient by selecting the VMAT technique because treatment time and MU of VMAT are less than the IMRT technique.

Table 6.2 The average scatter photon and neutron equivalent surface doses measured on the head, cervical, thoracic, abdominal, and pelvic regions with 3 the treatment techniques in the unit of mSv/Gy for 10 prostate cancer treatment cases

Region	3D (mSv/Gy)		IMRT(mSv/Gy)		VMAT(mSv/Gy)	
	Photon	Neutron	Photon	Neutron	Photon	Neutron
Head	1.71±0.08	0.12±0.01	1.92±0.08	0.21±0.01	1.87±0.08	0.16±0.01
Cervical	1.62±0.07	0.13±0.01	2.65±0.10	0.24±0.01	2.07±0.09	0.18±0.01
Thoracic	4.85±0.24	0.21±0.01	6.36±0.26	0.51±0.02	3.78±0.12	0.28±0.01
Abdominal	6.94±0.28	0.26±0.02	10.17±0.33	0.63±0.03	6.56±0.28	0.31±0.01
Pelvic	647.11±19.41	1.20±0.04	254.62±7.64	2.10±0.05	292.715±7.86	1.60±0.03

For the scatter photon equivalent doses, the photon dose per Gy also decreased further away from the in-field region. The scatter photon dose was highest in the case of 3D plan and in the pelvic region. This was because the measurement point was on the anterior position of the Rando phantom. The detectors were irradiated directly from the front in the 3D technique as opposed

to from other angles in the IMRT and VMAT techniques. On the other hand, the scatter photon doses from the IMRT were found to be highest in the out-of-field regions. They measured respectively 0.26, 0.63, and 0.31 mSv/Gy for the 3D, IMRT and VMAT at the abdomen surface region which was 20 cm from isocenter. The scatter photon dose depended on the beam irradiation time. It can scatter from the MLCs that closed for adjusting the dose. The IMRT plan consumed the highest MU per one treatment fraction. The scatter photon dose decreased further away from the isocenter. In the out-of-field region, the scatter photon equivalent doses were at least 10 times higher than the neutron equivalent dose.

6.2.2. Equivalent doses in the organs

The average scatter photon and neutron equivalent doses in 7 organs based on the 3 treatment techniques are shown in table 6.3. For all treatment techniques, the neutron equivalent doses at the bladder and the rectum were higher than at the other organs because their positions were within the in-field area. In all cases, the neutron doses from the IMRT plan were highest. The brain, which was the farthest from the isocenter, received less scatter photon and neutron doses than other organs. The scatter photon doses from the IMRT were also higher than from the other two techniques in most organs except for the bladder and the rectum. In the latter cases, the highest doses were from the 3D technique since the measurement points were on the anterior position on the Rando phantom, and the detectors faced the beam directly during the irradiation.

The neutron equivalent dose decreased several times in out-of-field organs in comparison to the in-field organs. Kry et al[5] estimated the neutron equivalent dose to each critical organ by using 15 MV for IMRT step-and-shoot technique. The neutron equivalent dose range was 2.5-9.0 µSv/MU in each organ. The value agreed well with our study. The equivalent doses from scatter photons were higher than from neutrons in all organs and treatment techniques.

The equivalent doses of neutron were 10% of those of scatter photon, but in several organs they could be as high as 20%.

Table 6.3 The average scatter photon and neutron equivalent doses measured in 7 organs with 3 treatment techniques in the unit of mSv/Gy for 10 prostate cancer treatment cases

Region	3D(mSv/Gy)		IMRT(mSv/Gy)		VMAT(mSv/Gy)	
	Photon	Neutron	Photon	Neutron	Photon	Neutron
Brain	1.65±0.07	0.10±0.01	3.91±0.12	0.20±0.01	1.86±0.07	0.16±0.01
Thyroid	1.87±0.08	0.13±0.01	4.44±0.13	0.28±0.01	2.01±0.08	0.22±0.01
Lung	2.11±0.08	0.28±0.01	6.52±0.15	0.41±0.02	2.76±0.08	0.39±0.02
Stomach	2.58±0.09	0.52±0.02	9.35±0.22	0.69±0.02	3.53±0.12	0.52±0.02
Liver	2.79±0.09	0.56±0.02	10.23±0.23	0.73±0.02	3.78±0.13	0.57±0.02
Bladder	150.25±4.52	0.61±0.02	80.56±2.24	0.82±0.03	78.88±2.22	0.65±0.02
Rectum	165.78±4.85	0.60±0.02	75.59±2.20	0.87±0.03	74.41±2.24	0.62±0.02

6.2.3 Effective dose

The effective dose of scatter photon and neutron were calculated and shown in table 6.4. The effective doses were computed from the equivalent dose of scatter photon and neutron. The effective doses were calculated from equivalent doses including all out-of-field organs and excluding the in-field organs (bladder and rectum). The equivalent dose multiplied by the tissue weighting factor and summed the dose of all out-of-field organs. The results illustrated that the IMRT technique yielded the highest effective dose from scatter photon and neutron with the total effective dose of 4.74 mSv/Gy. The total effective doses from the 3D and VMAT techniques were respectively 1.60 and 1.99 mSv/Gy, about 3 times less than the total effective dose of IMRT. In all

treatment technique, the effective doses from scatter photon were higher than from neutron.

Halg et al investigated the effective dose from the 3D, IMRT and VMAT techniques for treatment in the pelvic area using a Varian LINAC.[31] The effective doses were reported to be 1.90, 2.60, and 2.20 mSv/Gy respectively for the 3 techniques. The results for 3D and VMAT showed good agreement with our study. However, the result for IMRT was different because the number of monitor unit used for the IMRT plan in his study differed from the number in our study.

For prostate cancer cases, King Chualalongkorn Memorial hospital prescribed the total dose of 80 Gy. The total effective doses that exposed to patient during treatment per course were about 128, 379 and 160 mSv for 3D, IMRT and VMAT, respectively. The total effective dose are shown in table 6.5.

Table 6.4 The effective dose of scatter photon and neutron in 3D, IMRT and VMAT techniques.

Technique	Effective dose (mSv/Gy)		
	Scatter photon	Neutron	Total
3D	1.38	0.22	1.60
IMRT	4.43	0.31	4.74
VMAT	1.74	0.25	1.99

Table 6.5 The total effective dose of prostate cancer in 3D, IMRT and VMAT

Technique	Effective dose (mSv/80 Gy)
3D	128
IMRT	379
VMAT	160

CHAPTER 7
CONCLUSION

In this study, the neutron spectrum from the 15 MV photon beam has been investigated by the MCNP5 code. The dominant neutron flux is generated at the beam target. The neutron equivalent dose is between 3.45 to 9.75 mSv per photon Gy at the isocenter of the field. The neutron equivalent dose is found to be highest when the collimator jaws are fixed at 30x30 cm^2 and MLC is at 2x2 cm^2. At 100 cm out-of-field, the neutron dose is 10 times less than the dose in-field. The calculated and measured neutron doses are in agreement at every comparing position. The MCNP5 code can be effectively used to determine the neutron equivalent dose inside treatment room. This finding helps predict the neutron dose, and provide important information for determining radiation protection policy for patient and staff who work in the treatment room.

For the activation product study, the dominant activation product immediately after the irradiation is ^{28}Al. Since ^{28}Al is a short half-life isotope, protection against it can be easily implemented by allowing it to decay for a short period of time before entering the treatment room after the irradiation. For other isotopes that have longer half-lives, it is found that the personal gamma and neutron doses received are about 0.78 mSv/y and 0.60 mSv/y which are well within the recommended occupational dose limit of 20 mSv/y.[21] Thus, it is recommended that the therapist or staff should wait for a few minutes before entering the treatment room after irradiation, and stay only for a short period of time in the treatment room to minimize radiation exposure.

The scatter photon and neutron equivalent surface doses decreased further away from the in-field region. The neutron dose should be concerned when patients are treated by the photon energy higher than 10 MV because it can significantly generate photoneutrons inside the treatment room. The scatter photon and neutron equivalent doses vary with the treatment technique

employed. The IMRT technique, which consumes the highest MU per treatment fraction for the same prescribed dose, can generate higher neutron dose than other treatment techniques. Although the neutron dose from the VMAT technique is slightly higher than from the 3D technique, it is overall a better choice for treatment because it can decrease the neutron dose to patient while keeping the isodose coverage and ability to spare normal organ the same as the IMRT technique. The out-of-field organs are also exposed to neutrons, and in some cases the dose can be as high as 20% of the dose from scatter photons. This neutron dose can pose additional risk of secondary malignancy to the patient. If possible, the treatment energy of the photon beam should be selected to be less than 10 MV in order to reduce the unwanted dose and the risk of secondary malignancy to the patient and the treatment room staff.

The limitation of this study should be used the detector for neutron spectrum measurement to compare with the Monte Carlo simulation. For field size opened by MLCs, the equivalent dose should be measured at the closing MLCs position that it does not measure in this study. In the future work, the neutron equivalent dose should be measured by other detectors. The neutrons are very difficult for measurement because it varies the energy range. In each energy of neutron is suitable with different detectors for measurement.

REFERENCES

1.   Chibani O, Ma CM. Photonuclear dose calculations for high-energy photon beams from Siemens and Varian linacs. Medical physics. 2003;30(8):1990-2000.

2.   Nath A, Boyer A, La Rivirere P, Macall RC, Price KW. Neutron measurements around high energy X-ray radiotherapy machines. AAPM report No19. 1986.

3.   Followill D, Geis P, Boyer A. Estimates of whole-body dose equivalent produced by beam intensity modulated conformal therapy. International journal of radiation oncology, biology, physics. 1997;38(3):667-72.

4.   Reft CS, Runkel-Muller R, Myrianthopoulos L. In vivo and phantom measurements of the secondary photon and neutron doses for prostate patients undergoing 18 MV IMRT. Medical physics. 2006;33(10):3734-42.

5.   Kry SF, Salehpour M, Followill DS, Stovall M, Kuban DA, White RA, et al. Out-of-field photon and neutron dose equivalents from step-and-shoot intensity-modulated radiation therapy. International journal of radiation oncology, biology, physics. 2005;62(4):1204-16.

6.   Howell RM, Kry SF, Burgett E, Hertel NE, Followill DS. Secondary neutron spectra from modern Varian, Siemens, and Elekta linacs with multileaf collimators. Medical physics. 2009;36(9):4027-38.

7.   Zabihzadeh M, Ay MR, Allahverdi M, Mesbahi A, Mahdavi SR, Shahriari M. Monte Carlo estimation of photoneutrons contamination from high-energy X-ray medical accelerators in treatment room and maze: a simplified model. Radiation protection dosimetry. 2009;135(1):21-32.

8.   Nedaie H, Darestani H, Banaee N. Neutron dose measurements of Varian and Elektalinacs by TLD600 and TLD700 dosimeters and comparison with MCNP calculations. J Med Phys 2014;39(10-17).

9.   Passmore C, Kirr M. Neutron response characterization of an OSL neutron dosimeter. 2011;144:155-60.

10.   Martinez-Ovalle SA, Barquero R, Gomez-Ros JM, Lallena AM. Ambient neutron dose equivalent outside concrete vault rooms for 15 and 18 MV radiotherapy accelerators. Radiation protection dosimetry. 2012;148(4):457-64.

11.   Bednarz B, Xu XG. Monte Carlo modeling of a 6 and 18 MV Varian Clinac medical accelerator for in-field and out-of-field dose calculations: development and validation. Physics in medicine and biology. 2009;54(4):N43-57.

12.   Mao XS, Kase KR, Liu JC, Nelson WR, Kleck JH, Johnsen S. Neutron sources in the Varian Clinac 2100C/2300C medical accelerator calculated by the EGS4 code. Health physics. 1997;72(4):524-9.

13.   Fujibuchi T, Obara S, Sato H. Estimate of photonuclear reaction in a medical linear accelerator using a water-equivalent phantom. J NucSci Technol. 2011;2:803-7.

14.   Viamonte A, De Rosa L, Buckley L. Radiotherapy dosimetry using a commercial OSL system. Medical physics. 2008;34(5):1261-6.

15.   Yukihara E, Yoshimura E, Mardirossian G. High-precision dosimetry for radiotherapy using the Optically Stimulated Luminescence (OSL) technique and thin Al_2O_3:C dosimeter. 2005;50:5619-28.

16.   Rawlinson JA, Islam MK, Galbraith DM. Dose to radiation therapists from activation at high-energy accelerators used for conventional and intensity-modulated radiation therapy. Medical physics. 2002;29(4):598-608.

17.   Fischer H, Tabot B, Poppe B. Activation process in medical linear accelerators and spatial distribution of activation products. http://www.radioaktivitaet.uni-bremen.de/downloads/Fisch_pu1.pdf (19 February 2015, date last accessed).

18.   Almen A, Ahlgren L, Mattson S. Absorbed dose to technicians due to induced activity in linear accelerators for radiation therapy. Physics in medicine and biology. 1991;36:815-22.

19.   Powell NL, Newing A, Bullen MA, Sims C, Leaton SF. A radiation safety survey on a Clinac-20 linear accelerator. Physics in medicine and biology. 1987;32(6):707-18.

20.   LaRiviere PD. Radiotherapy technologist dose from high-energy electron medical accelerators. Health physics. 1985;49(6):1105-14.

21.   ICRP International Commission on Radiological Protection. The 2007 Recommendations of the International Commission on Radiological Protection. ICRP Publication 103, 2007.

22.   Podgorsak EB. Radiation Oncology Physics: A Handbook for Teachers and Students. Vienna: International Atomic Energy Agency. 2005.

23.   National Council on Radiation Protection and Measurements. Risk Estimates for Radiation Protection. NCRP Report 115. Bethesda (MD): National Council on Radiation Protection and Measurements; 1993.

24.   Jaradat AK, Biggs PJ. Measurement of the neutron leakage from a dedicated intraoperative radiation therapy electron linear accelerator and a conventional linear accelerator for 9, 12, 15(16), and 18(20) MeV electron energies. Medical physics. 2008;35(5):1711-7.

25.   Cygler J, Yukihara E. AAPM 51th annual meeting in 2009: United State. https://www.aapm.org/meetings/09SS/documents/25Cygler-OSL.pdf (17 April 2015, date last accessed).

26.   Bucci MK, Bevan A, Roach M, 3rd. Advances in radiation therapy: conventional to 3D, to IMRT, to 4D, and beyond. CA: a cancer journal for clinicians. 2005;55(2):117-34.

27.   Howell RM, Ferenci MS, Hertel NE, Fullerton GD, Fox T, Davis LW. Measurements of secondary neutron dose from 15 MV and 18 MV IMRT. Radiation protection dosimetry. 2005;115:508-12.

28.   Kry SF, Howell RM, Salehpour M, Followill DS. Neutron spectra and dose equivalents calculated in tissue for high-energy radiation therapy. Medical physics. 2009;36(4):1244-50.

29.   Howell RM, Hertel NE, Wang Z, Hutchinson J, Fullerton GD. Calculation of effective dose from measurements of secondary neutron spectra and scattered photon dose from dynamic MLC IMRT for 6 MV, 15 MV, and 18 MV beam energies. Medical physics. 2006;33(2):360-8.

30.   Aoyama T, Iguchi T, Miyata M, Ogata Y. Evaluation of neutron dose to radiotherapy patients treated with 10 MV x-ray beams based on photoneutron spectrometry. Jpn J Health phys. 2004;39(2):130-7.

31.   Halg RA, Besserer J, Schneider U. Systematic measurements of whole-body imaging dose distributions in image-guided radiation therapy. Medical physics. 2012;39(12):7650-61.

APPENDIX

APPENDIX A

The data of simulation of LINAC head for neutron calculated at 100 cm off axis by 10x10 cm^2 field size in standard FORTRAN-90 Programming Language and the actual LINAC geometry.

```
c cell# mat# density surface params.
   1   1    -19.3   -10    imp:n,p=1  $ Target W
   2   2    -0.001205 -20 10 50   imp:n,p=1   $ Gap target&pricoll
   3   1    -19.3   -30 10 20 50 60  imp:n,p=1  $ pricoll
   4   2  -0.001205  -40 10 20 30 50 60 70 115 117 119 &
120 121 122 123 124 125 126   imp:n,p=1  $ borndary
   5   0     40     imp:n,p=0
   6   3   -8.96 -50 10  imp:n,p=1   $ Target CU
   7   2    -0.001205  -60  imp:n,p=1     $ Beam track
   8   3   -8.96  -70   imp:n,p=1    $ Flattening
  26   1   -19.3  -115 116  imp:n,p=1         $ Upper Jaw Y
  27   2   -0.001205  -116  imp:n,p=1        $ Open Field Y
  28   1   -19.3  -117 118  imp:n,p=1          $ Lower Jaw X
  29   2   -0.001205  -118  imp:n,p=1        $ Lower Field x
  30   4   -7.874  -119   imp:n,p=1          $ Upper cover
  31   4   -7.874  -120   imp:n,p=1          $ Right Shield X
  32   4   -7.874  -121   imp:n,p=1          $ Left Shield X
  33   4   -7.874  -122   imp:n,p=1          $ Right Shield Y
  34   4   -7.874  -123   imp:n,p=1          $ Left Shield Y
  35   5   -0.998207  -124 125   imp:n,p=1     $ Water Phantom
  36   5   -0.998207  -125   imp:n,p=1     $ ion chamber
  38   6   -2.32  -126   imp:n,p=1          $ Floor


c surface card
10  RPP -2 2  -2 2  -0.1 0
20  RPP -2.5 2.5  -2.5 2.5  -1.6 0
30  RPP -4 4  -4 4  -7.6 0
```

```
40  SO   250
50  RPP  -2 2 -2 2  -0.9 0
60  TRC  0 0 -1.6   0 0 -6   0.399   1.895
70  TRC  0 0 -10.92764   0 0 -0.744   0  3.85
115  RPP  -10 10  -10 10  -35.8 -28
116  RPP  -10 10  -1.6 1.6  -35.8 -28
117  RPP  -11 11  -11 11  -44.5 -36.7
118  RPP  -1.9 1.9 -11 11  -44.5 -36.7
119  RPP   -16 16  -16 16  5 12
120  RPP  16 23  -16 16  -45 12
121  RPP  -23 -16  -16 16  -45 12
122  RPP  -16 16  16 23  -45 12
123  RPP  -16 16  -23 -16  -45 12
124  RPP  -30 30  -30 30  -150 -100
125  RCC  0 -101.25 -105  0 2 0  10
126  RPP  -50 50  -50 50  -230 -220
c material
mode p n
SDEF PAR=1 ERG=d2 POS=0 0 0
SI2  H 0 1.00E-04 5.88E-01 1.18E+00 1.76E+00 2.35E+00 2.94E+00 &
 3.53E+00 4.12E+00 4.71E+00 5.29E+00 5.88E+00 6.47E+00 7.06E+00 &
 7.65E+00 8.24E+00 8.82E+00 9.41E+00 1.00E+01 1.06E+01 1.12E+01 &
 1.18E+01 1.24E+01 1.29E+01 1.35E+01 1.41E+01 1.47E+01
SP2  0 75.52046898  430889779  4.532707733  2.89907591 1.9479854 &
  1.37534403 1.028147846 0.788811551 0.628124282 0.518245739 &
  0.4240487 0.357966073 0.299403721 0.254322835 0.219676585 &
  0.182066043 0.153146615 0.126295771 0.101859669 0.078555073 &
  0.059153173 0.039394722 0.022815473 0.009497118 0.001834213 &
  0.000163041
M1  74000  -1   $ Tungsten
M2  6000  -0.000124  7014  -0.755268  8016  -0.231781  18000  -0.012827  $ Air
M3  29000  -1   $ Cu
```

M4 26000 -1 $ Lead

M5 1001 -0.111894   8016 -0.888106 $ Water

M6 1001 -0.01 8016 -0.532 11023 -0.029   13027 -0.034

    14000 -0.337   20000 -0.044 26000 -0.014

F4:n 36

DE4 2.5E-8 1.0E-7 1.0E-6 1.0E-5 1.0E-4 1.0E-3 1.0E-2 1.0E-1 0.5 1 2 &

5 10 20

DF4 3.85E-6 4.17E-6 4.55E-6 4.35E-6 4.17E-6 3.70E-6 3.57E-6 2.08E-5 &

7.14E-5 1.18E-4 1.43E-4 1.47E-4 1.47E-4 1.54E-4

nps 10000000

 Actual geometry of Linear accelerator.
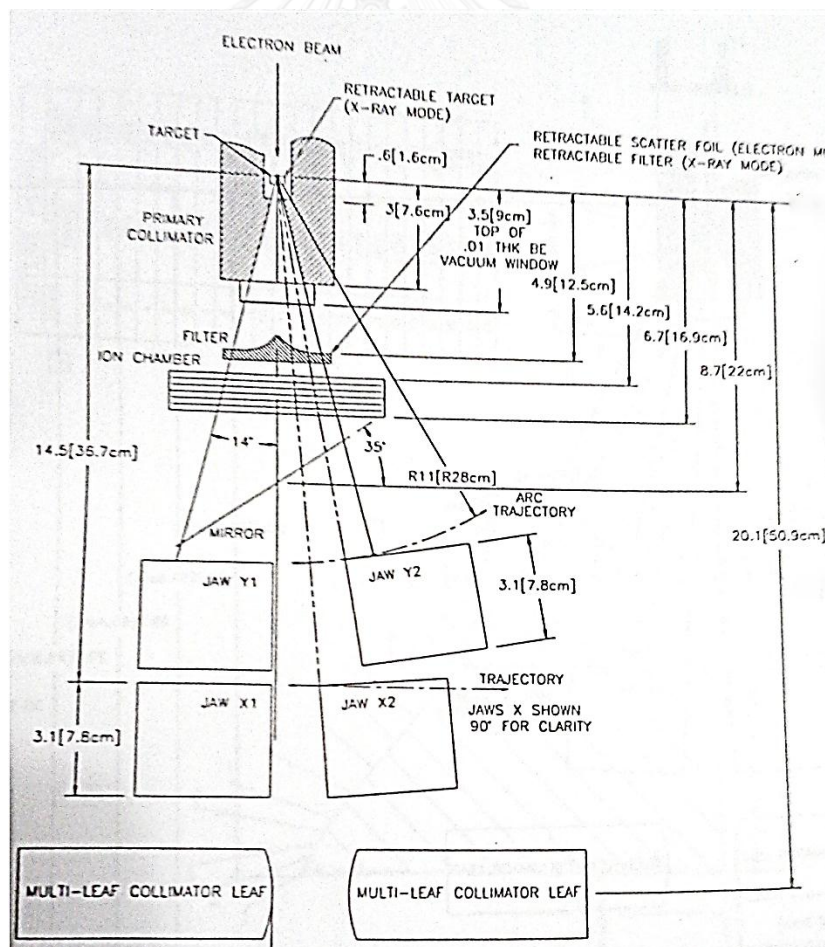
Materials of LINAC head components

Components	Materials
Target	Tungsten + Copper
Primary collimator	Tungsten
Flattening filter	Aluminium
Secondary collimator	Tungsten
MLCs	Tungsten

APPENDIX B

The data of neutron dose equivalent using OSL measurement in 5 times for different field sizes.

Field size (cm^2)	Measurement (mSv/Gy)				
2x2	3.82	3.75	3.78	3.85	3.74
5x5	3.97	4.01	4.17	4.13	4.15
10x10	5.35	5.33	5.47	5.41	5.38
15x15	5.54	5.7	5.57	5.65	5.61
30x30	6.66	6.85	6.79	6.68	6.75

APPENDIX C

The data of neutron dose equivalent using OSL measurement in 5 times for different SSD.

SSD (cm)	Measurement				
	(mSv/Gy)				
80	7.35	7.5	7.48	7.4	7.52
100	5.27	5.45	5.41	5.32	5.38
150	4.34	4.3	4.24	4.38	4.21
200	2.29	2.39	2.51	2.45	2.33

APPENDIX D

The data of neutron dose equivalent using OSL measurement in 5 times at in-field and out of field distance.

Distance (cm)	Measurement (mSv/Gy)				
Isocenter	5.41	5.28	5.44	5.47	5.35
100	0.42	0.31	0.45	0.36	0.55
150	0.31	0.16	0.11	0.21	0.28
200	0.15	0.08	0.13	0.18	0.21

APPENDIX E

The data of neutron dose equivalent using OSL measurement in 5 timesfor different field size opened by MLCs.

Field size (cm^2)	Measurement (mSv/Gy)				
2x2	9.85	9.63	9.77	9.82	9.69
5x5	7.05	7.12	6.97	6.95	7.09
10x10	5.09	4.86	4.97	5.04	5.01
15x15	4.31	4.19	4.36	4.41	4.33

VITA

NAME	Mr. IsraIsrangkul Na Ayuthaya
SEX	Male
NATIONALITY	Thai
DATE OF BIRTH	17 September 1981
PLACE OF BIRTH	Bangkok, Thailand
INSTITUTIONS ATTENDED	Mahidol University, 2003
	Bechelor of Science
	(Radiological Technology)
	Mahidol University, 2005
	Master of Science
	(Medical Physics)
	Chulalongkorn University, 2015
	Doctoral of Engineering
	(Nuclear Engineering)
HOME ADDRESS	2 BanbuSirirajBangkoknoi
	Bangkok, Thailand 10700
	Tel. +66-866115996